

# Nano-HTDMA for investigating hygroscopic properties of sub-10 nm aerosol nanoparticles

Ting Lei<sup>1,2</sup>, Nan Ma<sup>4,1,3</sup>, Juan Hong<sup>4,1</sup>, Thomas Tuch<sup>3</sup>, Xin Wang<sup>2</sup>, Zhibin Wang<sup>5</sup>, Mira Pöhlker<sup>2</sup>, Maofa Ge<sup>6</sup>, Weigang Wang<sup>6</sup>, Eugene Mikhailov<sup>7</sup>, Thorsten Hoffmann<sup>8</sup>, Ulrich Pöschl<sup>2</sup>, Hang Su<sup>2</sup>, Alfred Wiedensohler<sup>3</sup>, Yafang Cheng<sup>1</sup>

<sup>1</sup>Minerva Research Group, Max Planck Institute for Chemistry, 55128 Mainz, Germany

<sup>2</sup>Multiphase Chemistry Department, Max Planck Institute for Chemistry, 55128 Mainz, Germany

<sup>3</sup>Leibniz Institute for Tropospheric Research, 04318 Leipzig, Germany

<sup>4</sup>Institute for Environmental and Climate Research, Jinan University, 511443 Guangzhou, China

<sup>5</sup>Reserch Center for Air Pollution and Health, College of Environmental and Resource Science, Zhejiang University, Hangzhou, 310058, China

<sup>6</sup>Beijing National Laboratory for Molecular Sciences (BNLMS), Institute of Chemistry, Chinese Academy of Sciences, Beijing, 100190, P. R. China

<sup>7</sup>St. Petersburg State University, 7/9 Universitetskaya nab., St. Petersburg, 199034, Russia

<sup>8</sup>Institute of Inorganic Chemistry and Analytical Chemistry, Johannes Gutenberg University Mainz, Mainz, Germany

*Correspondence to:* Yafang Cheng ([yafang.cheng@mpic.de](mailto:yafang.cheng@mpic.de)) and Juan Hong ([juanhong0108@jnu.edu.cn](mailto:juanhong0108@jnu.edu.cn))

**Abstract.** Interactions between water and nanoparticles are relevant for atmospheric multiphase processes, physical chemistry, and materials science. Current knowledge of the hygroscopic and related physico-chemical properties of nanoparticles, however, is restricted by limitations of the available measurement techniques. Here, we present the design and performance of a nano-hygroscopicity tandem differential mobility analyzer (nano-HTDMA) apparatus that enables high accuracy and precision in hygroscopic growth measurements of aerosol nanoparticles with diameters less than 10 nm. Detailed methods of calibration and validation are provided. Besides maintaining accurate and stable sheath/aerosol flow rates ( $\pm 1\%$ ), high accuracy of DMA voltage ( $\pm 0.1\%$ ) in the range of  $\sim 0$ -50 V is crucial to achieve accurate sizing and small sizing offsets between the two DMAs ( $< 1.4\%$ ). To maintain a stable relative humidity (RH), the

humidification system and the second DMA are placed in a well-insulated and air conditioner housing ( $\pm 0.1\text{K}$ ). We also tested and discussed different ways of preventing pre-deliqescence in the second DMA. Our measurement results for ammonium sulfate nanoparticles are in good agreement with Biskos et al. (2006b), with no significant size-effect on the deliquescence and efflorescence relative humidity (DRH, ERH) at diameters down to 6 nm. For sodium sulfate nanoparticles, however, we find a pronounced size-dependence of DRH and ERH between 20 and 6 nm nanoparticles.

34

## 35 **1 Introduction**

The climatic effects of aerosol nanoparticles have attracted increasing interests in recent years (Wang et al., 2016; Andreae et al., 2018; Fan et al., 2018). Interactions between water and nanoparticles are relevant for atmospheric multiphase processes, physical chemistry, and materials science (Zheng et al., 2015; Cheng et al., 2015, 2016). Aerosol nanoparticles in the atmosphere are mostly originating from new particle formation, and a fraction of these nanoparticles could potentially grow into sizes to efficiently act as cloud condensation nuclei and thus to change the contributions of aerosol nanoparticles to climate forcing (Lihavainen 2003; Wiedensohler et al., 2009; Sihto et al., 2011; Kirkby et al., 2011; Keskinen et al., 2013; Dunne et al., 2016; Kim et al., 2016). These processes strongly depend on the chemical composition and physico-chemical properties of these nanoparticles (Köhler, 1936; Su et al., 2010; Wang et al., 2015; Cheng et al., 2015). One of the most important physico-chemical properties of nanoparticles is their hygroscopic behavior that describes their ability to take up water, and it can differ significantly from that of larger particles (Hämeri et al., 2000, 2001; Gao et al., 2006; Biskos et al., 2006a, b, 2007; Cheng et al., 2015).

To understand and predict hygroscopic properties of nanoparticles, current thermodynamic models mostly rely on the concentration-dependent thermodynamic properties (such as water activity and interfacial energy) derived from the measurements of large aerosol particles or even bulk samples (Tang and Munkelwitz, 1994; Tang 1996; Pruppacher and Klett, 1997; Clegg et al., 1998). They are thus difficult or

impossible to be applied to describe the hygroscopic behavior of sub-10 nm nanoparticles which can be often supersaturated in concentration compared to bulk solutions (Cheng et al., 2015). Furthermore, the nanosize effect on these properties may also need to be considered (Cheng et al., 2015). The lack of such data hinders the understanding and an accurate simulation of the interaction of water vapor and atmospheric nanoparticles. In addition, by knowing the hygroscopicity of newly formed nanoparticle, one can infer the involving chemical species (e.g., organic ratio) in particle formation and initial growth (Wang et al., 2010), which is otherwise difficult and highly challenging to measure directly (Wang et al., 2010; Ehn et al., 2014). Hence, to measure the hygroscopicity of nanoparticles is essential to improve our understandings of aerosol formation, transformation, and their climate effects.

Different techniques have been employed to characterize the hygroscopic properties of aerosol particles in different sizes (Fig. S1) (Tang et al., 2019), such as Fourier transform infrared spectrometer (FT-IR) (Zhao et al., 2006), Raman spectroscopy (Dong et al., 2009), electrodynamic balance (EDB) (Chan and Chan, 2003, 2005; Chan et al., 2008), optical tweezers (Reid et al., 2011; Rickards et al., 2013), hygroscopicity tandem differential mobility analyzer (HTDMA) (e.g., Rader and McMurry, 1986; Mikhailov et al., 2004; 2008; 2009; Biskos et al., 2006a, b, 2007; Cheng et al., 2008, 2009; Eichler et al., 2008; Stock et al., 2011; Hong et al., 2014, 2015; Lei et al., 2014; 2018; Mikhailov and Vlasenko, 2019), and atomic force microscopy (AFM) (Estill et al., 2017). Using these techniques, most of the early lab studies focus on the hygroscopic behavior of particles in accumulation modes and super-micron size range, including deliquescence, efflorescence of pure components and the effect of organics on the change or suppression of deliquescence and efflorescence of these inorganic components in mixtures.

For nanoparticles with diameters down to sub-10 nm, there are, however, only very few studies attempting to investigate their interactions with water molecules, which mainly utilized the setup with humidified tandem DMAs (Hämeri et al., 2000, 2001; Sakurai et al., 2005; Biskos et al., 2006a, b, 2007; Giamarelou et al., 2018). In Table S1, we summarized the measured DRH and ERH of ammonium sulfate nanoparticles

76 in the size range from 6 to 100 nm using HTDMAs. In these studies, the results of the observed  
77 deliquescence and efflorescence relative humidity (respective DRH and ERH) and prompt or non-prompt  
78 phase transitions of ammonium sulfate nanoparticles, however, do not show universal agreement. The  
79 technical challenges in HTDMA measurements, especially in the sub-10 nm size range, mainly lie on: (1)  
80 accurate sizing and small sizing offset of the two DMAs, (2) highly stable measurement conditions in the  
81 whole system. Large sizing offset between the two DMAs may lead to significant error in the measured  
82 growth factor based on error propagation (Mochida and Kawamura, 2004). Massling et al. (2011) and  
83 Zhang et al. (2016) suggested that to achieve good hygroscopic growth factor of nanoparticles, the sizing  
84 offset of the two DMAs should be within  $\pm 2\text{-}3\%$ , which is however very difficult to maintain for the sub-  
85 10 nm size range. To accurately measure phase transition (e.g., DRH and ERH), a highly stable  
86 measurement condition is essential, especially maintaining a small temperature perturbation in the  
87 humidification system and inside the second DMA to prevent pre-deliqescence. For example, a 0.8 K  
88 fluctuation of the experimental temperature during the measurement can result in a 4% difference in RH  
89 (0-90%) inside the humidified DMA (Hämeri et al., 2000), leading to an inaccurate determination of the  
90 phase transition. Another problem is the prompt versus non-prompt phase transition. Although effects of  
91 impurities on the phase transition of aerosol nanoparticles (Biskos et al., 2006a; Russell and Ming, 2002)  
92 may be one possible reason of the previously observed non-prompt phase transitions (e.g., Hämeri et al.,  
93 2000), the apparent non-prompt phase transition of aerosol nanoparticles has been thought to be mainly due  
94 to the inhomogeneity of RH and temperature in the humidified DMA during measurements (Biskos et al.,  
95 2006b; Bezantakos et al., 2016). Moreover, the hygroscopic measurements are in general difficult for  
96 nanoparticles with diameters below 20 nm due to high diffusion losses of nanoparticles (Seinfeld and  
97 Pandis, 2006).

98 In this study, we present a design of nano-HTDMA setup that enables high accuracy and precision in  
99 hygroscopic growth measurements of aerosol nanoparticles with diameters less than 10 nm. Detailed  
100 methods of calibration and validation are provided. We discuss in detail how to maintain the good

performance of the system by minimizing uncertainties associated with the stability and accuracy of RH, temperature, voltage for nanoparticle classification, and sheath and aerosol flows in the DMA systems. We then apply the nano-HTDMA system to study the size dependence of the deliquescence and the efflorescence of aerosol nanoparticles of two specific inorganic compounds (e.g., ammonium sulfate and sodium sulfate) for sizes down to 6 nm.

## 2. Methods

### 2.1 Nano-HTDMA system

A nano-HTDMA system is built up to measure the aerosol nanoparticle hygroscopic growth factor ( $g_f$ ), especially aiming for accurate measurement of phase transition and hygroscopic growth factor for nanoparticles in the sub-10 nm size range. Here,  $g_f$  is defined as the ratio of mobility diameters of nanoparticles after humidification ( $D_m(RH)$ ) to that at dry condition ( $D_m(< 10\% RH)$ ) (see SI. S1. Eq. (S1)). As presented in Fig. 1, the nano-HTDMA composes three main components, including two nano-differential mobility analyzers (nano-DMA, TROPOS Model Vienna-type short DMA; Birmili et al., 1997), an ultrafine condensation particle counter (CPC, TSI Model 3776), and a humidification system. Table 1 shows the technical specification, where the DMA system, humidification system, and temperature system of the three HTDMAs setup are compared among the systems of Biskos et al. (2006b), Hämeri et al. (2000) and this study.

In our setup (Fig. 1), the first nano-DMA (nano-DMA1) is used to produce quasi-monodisperse nanoparticles at a desired dry diameter. The flow rate of the closed-loop sheath flow in the nano-DMA1 is maintained at 10 l/min. The ratio of sheath flow to aerosol flow is 10:1.5. The sheath flow is dried to RH below 10% by two custom-built Nafion dryers (TROPOS Model ND.070) in parallel. The quasi-monodisperse nanoparticles produced by nano-DMA1 then enter the humidification system, which can be

124 set to deliquescence mode (from low RH to high RH for measuring deliquescence) or efflorescence mode  
125 (from high RH to low RH for measuring efflorescence). In the deliquescence mode, dry nanoparticles are  
126 humidified by a Nafion humidifier (NH-1, TROPOS Model ND.070, L. 24") to a target RH. In the  
127 efflorescence mode, nanoparticles are first exposed to a high RH condition (~97% RH) in a Nafion  
128 humidifier (NH-2, Perma Pure Model MH-110, L. 12") and then dried to a target RH through NH-1. The  
129 humid flow in the outer tube of NH-1 is a mixture of high-humidity air produced with a custom-built Gore-  
130 Tex humidifier and heater (GTHH: TROPOS Model Di. 0.6", L. 11.8") and dry air in variable proportions.  
131 To have a precise control of the aerosol RH, the flow rates of the humid and dry air are adjusted with a  
132 proportional-integral-derivative (PID) system, including two mass flow controllers (MFC: MKS Model  
133 MF1) and a RH sensor (Vaisala Model HMT330) downstream of NH-1.

134 The residence time is ~5.4 s in the NH-1 for both the deliquescence and the efflorescence modes. Many  
135 groups have reported that the residence time of a few seconds is sufficient to reach equilibrium for  
136 measuring hygroscopic growth or shrink of inorganic salt particles, e.g., ammonium sulfate and chloride  
137 sodium (Chan and Chan, 2005; Duplissy et al., 2009; Lei et al., 2014, 2018; Giamarelou et al., 2018). More  
138 specifically, Kerminen (1997) estimated the time for reaching the water equilibrium to be between  $8 \times 10^{-6}$   
139 s and 0.005 s for 100 nm nanoparticles at 90% RH at 25°C with accommodation coefficients from 0.001  
140 to 1, respectively. In our study, we measured the inorganic aerosol nanoparticles with diameters from ~100  
141 nm down to 6 nm, thus the equilibrium time should be even shorter as nanoparticle size decreases (Table.  
142 S2). In NH-2, the residence time is ~0.07 s for the deliquescence of inorganic aerosol nanoparticles at very  
143 high RH condition (~97% RH), which is much longer than the time estimated for phase transition by  
144 Duplissy et al. (2009) (in the order of a few milliseconds) and Raoux et al. (2007) (in the order of a few  
145 nanoseconds). In addition, we have tested a longer NH-2 (Perma Pure Model MH-110, L. 48") in the  
146 efflorescence mode, and no significant difference in measured growth factors are found, indicating that the  
147 residence time in NH-1 and NH-2 should be sufficient.

148 The number size distribution of the humidified nanoparticles is measured with a combination of the second  
149 nano-DMA (nano-DMA2) and the ultrafine CPC. Similar to Biskos et al. (2016b), a multiple Nafion  
150 humidifier (NH-3, Pure Model PD-100) is used in our nano-HTDMA system to rapidly adjust the RH of  
151 the sheath flow of nano-DMA2. The sheath flow is fed into the outer tube of NH-3 to minimize its pressure  
152 drop. The RH of humid flow in the inner tube of NH-3 is controlled with a similar PID system as that for  
153 NH-1. A RH sensor (Vaisala Model HMT330) downstream of NH-3 is used to provide feedback to the PID  
154 system. In our nano-HTDMA system, a dew point mirror (DPM: EDGE TECH Model MIRROR-99) is  
155 placed in the excess flow line to measure the RH and temperature of excess flow of the nano-DMA2. During  
156 the operation, the difference between sheath flow RH and aerosol flow RH has been maintained within  
157  $\pm 1\%$  (see more details in Section 2.2).

158 The sheath flow is maintained to the set flow rate with a PID-controlled recirculation blower (RB:  
159 AMETEK Series MINISPIRAL). Prior to every size scan, the sheath flow rate of nano-DMA2 is adjusted  
160 by the PID system according to the measurement of a mass flow meter (MFM: TSI Series 4000) in the  
161 sheath flow line. In order to minimize the pressure drop along the recirculating sheath flow loop, low flow  
162 resistance MFM and hydrophobic filter (HF: Whatman Model 6702-3600) are used. A heat exchanger (HE,  
163 Ebmpapst Model 4414FM) is installed downstream of the RB to minimize the temperature perturbation in  
164 the sheath flow by the heat generated in the RB.

165 As aforementioned, temperature non-uniformity is the main contributor to the fluctuation of RH within  
166 humidified DMA. Temperature difference within nano-DMA2 is unavoidable mainly due to temperature  
167 difference between inner electrode and the rest of nano-DMA2 parts and/or the temperature difference  
168 between aerosol and sheath flow (Duplissy et al., 2009; Bezantakos et al., 2016). As shown in Fig. 1, to  
169 investigate and monitor the temperature difference within nano-DMA2 during measurements, a  
170 temperature sensor (THERMO ELECTRON Model Pt100) is placed at the inlet of the sheath flow and the  
171 temperature of sheath excess flow is monitored by the DPM. Note that, a DPM should be installed as close

as possible to the nano-DMA2 in the excess flow, which better represents the conditions inside the nano-DMA2, such as temperature and RH (Wiedensohler et al., 2012). In addition, the temperature of aerosol flow is monitored at the inlet of the aerosol flow of nano-DMA2.

Moreover, to maintain a stable environment that required for the growth factor measurements, nano-DMA2 with its sheath flow humidification system is placed in a well-insulated housing chamber (marked with yellow dashed lines in Fig. 1). An air conditioner (Telemeter Electro Model TEK-1004-RR-24-IP55) is installed inside the housing to maintain a constant temperature ( $292.15 \pm 0.1$  K), which is set to be  $\sim 1$  K lower than the constant laboratory temperature (293 K) in order to achieve high RH ( $\sim 90\%$ ) inside nano-DMA2.

## 2.2 Calibration of nano-HTDMA

The purpose of this study is to design and build a nano-HTDMA system that is able to measure the hygroscopic properties of nanoparticles, especially in the sub-10 nm size range. A small perturbation in the measurement conditions may lead to large biases in the results. Hence, to provide high quality hygroscopicity measurements of nanoparticles, systematic calibration of the nano-HTDMA should be conducted regularly to ensure the accuracy and stability of the measurement conditions. Table 1 lists the possible sources of uncertainty, which could affect the performance of the HTDMAs. In our setup, nanoparticle sizing, aerosol/sheath flow rates, the high voltage (HV) applied to nano-DMAs, RH sensors, and temperature sensors are calibrated and verified independently.

Note that in the following, for calibration and/or checking of different parameters, the criteria and/or standard that the nano-HTDMA system has to meet are listed mainly according to the suggestions from Duplissy et al., (2009) and Wiedensohler et al. (2012), which are not specifically provided for accurately measuring sizes or hygroscopic growth of sub-10 nm nanoparticles. Compared with these criteria, to measure hygroscopic growth of sub-10 nm nanoparticles, we have achieved a better condition for our nano-

195 HTDMA system after comprehensive calibrations described as follows (more details about performance of  
196 our system see section 3).

### 197 **2.2.1 Sizing accuracy**

198 For particle diameters higher than 100 nm, the verification of sizing accuracy of DMAs can be  
199 accomplished by using certified particles of known sizes such as polystyrene latex (PSL) spheres (Hennig  
200 et al., 2005; Mulholland et al., 2006; Duplissy et al., 2009; Wiedensohler et al., 2012, 2018). The particle  
201 sizing of nano-DMA2 is checked with PSL by switching off the sheath flow and the HV supply of nano-  
202 DMA1, which actually in this case does not function as a DMA, but rather a stainless-steel tube. Sizing  
203 agreement between measured diameters and nominal diameters of PSL particles above 100 nm should be  
204 within  $\pm 3\%$  (Wiedensohler et al., 2012). After confirming the accurate sizing of nano-DMA2, the sizing  
205 accuracy of nano-DMA1 can be in turn checked by the nano-DMA2 with a full scan of a certain size of  
206 PSL selected by the nano-DMA1. Note that, it is important to check not only the sizing accuracy of both  
207 DMAs, but also the sizing agreement between the nano-DMA1 and nano-DMA2. To achieve good  
208 hygroscopicity measurements of nanoparticles, the sizing offset of the two DMAs should be within  $\pm 2-3\%$   
209 (Massling et al., 2011; Zhang et al., 2016).

210 For nanoparticles with diameters smaller than 100 nm, the sizing accuracy is, however, difficult to check  
211 by using PSL nanoparticles. This is mainly because the size of residual material in the solution also peaks  
212 around 20 – 30 nm (Fig. S2a), resulting in an asymmetric number size distribution of generated PSL  
213 nanoparticles (Fig. S2b) (Wiedensohler et al., 2012). PSL nanoparticles with diameters below 20 nm are  
214 not commercially available (<https://www.thermofisher.com/order/catalog/product/3020A>), making the  
215 verification in this size range even impossible. Sizing accuracy of nanoparticles is critically determined by  
216 sheath flow rates and HV applied to the nano-DMAs. However, unlike for the 100 nm nanoparticles, a  $\pm 2-$   
217  $3\%$  sizing offset between the two DMAs would be very difficult to maintain for nanoparticles with  
218 diameters smaller than 20 nm. Thence, accurate calibrations of sheath flow rates and high voltage are crucial

for constraining the uncertainty associated with sizing of nanoparticles below 100 nm. The calibrations for aerosol/sheath flow, DMA voltage, and sensors will be described in detail in the following Section 2.2.2-2.2.5.

### **2.2.2 Aerosol and sheath flow**

Sizing accuracy of a DMA directly depends on the accuracies of aerosol and sheath flow rates. The aerosol flow rate at the inlet of the nano-DMA1 is checked by using a bubble flow meter (Gilian Model Gilibrator-2). Wiedensohler et al. (2012) recommended that the measured aerosol flow rate should not deviate more than 5% from the set flow rate during the measurements, otherwise one should check the flow rate of CPC or if there is a leakage in the system. Details about leakage checking can be found in Birmili et al. (2016).

To calibrate the sheath flow, a verified MFM (TSI Series 4000) is placed in the recirculating sheath flow close-loop upstream of the MFM. By applying a series of sheath flow rates, a calibration curve (flow rate vs. MFM analogue output) can be obtained according to the reading of the reference MFM. Maximum deviation of 2% from the sheath flow rate value of the reference MFM is recommended by Wiedensohler et al. (2012), which can keep sizing accuracy of 200 nm PSL particles within  $\pm 2\%$ .

### **2.2.3 DMA voltage**

The sizing of nano-DMAs is very sensitive to the accuracy and precision of the voltages applied, especially when measuring nanoparticles in the sub-10 nm diameter range. A verified reference voltage meter with voltage up to 1000 V (Prema Model 5000 DMM, accuracy 0.005%) is used to calibrate the HV supply of the nano-DMAs (0-350 V). By setting a series of analogue voltage values, the HV applied to nano-DMA can be calibrated according to the values shown in the reference voltage meter. For our nano-DMAs, sub-10 nm in particle sizes correspond to voltage below 50 V. Thence, voltage calibration should be performed with a higher resolution (smaller voltage interval) from 0 to 50 V (shown in the insert of Fig. 2).

### **2.2.4 RH sensor**

One typical method to calibrate RH sensors in a HTDMA system is to measure the hygroscopic growth factors of ammonium sulfate (Hennig et al., 2005), although the effects of shape factors, restructuring, and impurities in the solutions may hamper a reliable RH calibration with this method (Duplissy et al., 2009). Moreover, this indirect RH sensor calibration through measurement of the hygroscopic growth factors of ammonium sulfate (usually with nanoparticle diameters around or above 100 nm) only calibrates the RH values higher than the ERH of the pure salt. Calibration of RHs below ERH of ammonium sulfate is important for the phase transition measurements. Most importantly, we are investigating the hygroscopic growth factors of ammonium sulfate nanoparticles. Hence, using ammonium sulfate nanoparticles to calibrate RH sensors in our system becomes invalid.

Therefore, we alternatively calibrate the RH sensors by using a DPM (EDGE TECH Model MIRROR-99), which is recommended in several previous studies (Hennig et al., 2005; Duplissy et al., 2009; Biskos et al., 2006a, b, 2007). In the calibration, the DPM and RH sensors should be kept in the well-insulated chamber with constant laboratory conditions (e.g., flow rates, temperature, and pressure). By running the DPM and all the other RH sensors in parallel at various RHs (5% to 90%), a calibration curve of the RHs measured by the DPM against analogue voltages of RH sensor can be obtained.

#### **2.2.5 Temperature sensor**

Since all our temperature sensors and the high accurate DPM (EDGE TECH Model MIRROR-99) are installed in the aforementioned well-insulated chamber and the chamber temperature is maintained with air conditioner at about  $292.15 \pm 0.1$  K, we calibrate the temperature sensors and corrected their systematic shift by comparing the record of temperature sensors and the DPM by keeping them in parallel inside the chamber over a 12-hour time period.

#### **2.3 Particle generation**

264 The experiments shown in this study were conducted using laboratory generated ammonium sulfate and  
265 sodium sulfate nanoparticles. Nanoparticles with diameters of 6, 8, and 10 nm were generated by an  
266 electrospray (AG: TSI Model 3480) with 1, 5, and 20 mM aqueous solution of ammonium sulfate and  
267 sodium sulfate (Aldrich, 99.99%), respectively. The generated particles were then diluted and dried to RH  
268 below 2% by mixing with dry and filtered N<sub>2</sub> (1 l/min) and CO<sub>2</sub> (0.1 l/min). The dried polydisperse aerosol  
269 nanoparticles were subsequently neutralized by a Po<sup>210</sup> neutralizer. To avoid blocking the 25-μm capillary  
270 of the electrospray with high solution concentration, we used an atomizer (AG: TSI Model 3076) to  
271 generate nanoparticles with diameters of 60-100 nm and 20 nm with 0.05 and 0.001 wt% solution of  
272 ammonium sulfate and sodium sulfate (Aldrich, 99.99%), respectively. Also, 100-nm PSL nanoparticles  
273 were atomizing a PSL solution of mixing 3 drops of 100-nm PSL with 300 mL distilled and de-ionized  
274 milli-Q water. The generated nanoparticles were subsequently dried to RH below 10% with a custom-built  
275 Nafion dryer (ND: TROPOS Model ND.070) and then neutralized by a Kr<sup>85</sup> neutralizer.

276 The solutions used in our measurements were prepared with distilled and de-ionized milli-Q water  
277 (resistivity of 18.2 MΩ cm at 298.15 K). Note that, for 100-60 nm and 20 nm, the solution concentration  
278 was adjusted so that the sizes selected by the nano-DMA1 were always larger than the peak diameter of the  
279 number size distribution of the generated nanoparticles to minimize the influence of the multiple charged  
280 nanoparticles in hygroscopicity measurements. The influence of multiple charges on sub-10 nm particles  
281 is expected to be very small, we, however, still used different concentrations so that the sizes selected by  
282 the nano-DMA1 were always around the peak of the number size distribution of the generated nanoparticles  
283 by the electrospray (Fig. S3). This is to ensure that we could have as many particles as possible to  
284 compensate the strong loss of very small particles in the whole humidification systems.

285

## 286 **3 Results and discussion**

### 287 **3.1 Performance of the nano-HTDMA**

### 288 3.1.1 Sizing accuracy

289 In this section, we show the performance of our nano-HTDMA after a full calibration, including accuracy  
290 and stability of the aerosol/sheath flow rates, the voltage applied to the nano-DMA, and nanoparticle-  
291 sizing accuracy. In our study, the sheath/aerosol flow rates and nano-DMA voltage supply have been  
292 calibrated every day and every two weeks, respectively. The deviations of the measured aerosol/sheath flow  
293 rates from the set-point values are less than  $\pm 1\%$ , which is lower than the maximum variation of 2%  
294 recommended by Wiedensohler et al. (2012).

295 The voltage applied to the nano-DMA (up to 350 V) is kept within  $\pm 0.1\%$  around the set value shown in  
296 the voltage meter. As shown in Fig. 3a, when test with 100-nm PSL nanoparticles, the average peak  
297 diameter of scans from the nano-DMA2 is 100.4 nm, which matches well with the mean diameter of PSL  
298 nanoparticles ( $100 \pm 3$  nm, Thermo Fisher Scientific Inc.). Afterwards, when using nano-DMA1 select 100  
299 nm PSL, the scanned size distribution by nano-DMA2 has a peak diameter at 100.3 nm (Fig. 3b), indicating  
300 a good sizing accuracy of the nano-DMA1 too. As discussed in Sec. 2.2.1, it is difficult to verify the sizing  
301 accuracy of sub-100 nm aerosol nanoparticles using PSL nanoparticles. Duplissy et al. (2009) and  
302 Wiedensohler et al. (2012) suggested to estimate the sizing accuracy of sub-100 nm nanoparticles through  
303 DMA transfer function. The theoretical DMA transfer function (see SI. S2. Eq. (S2-S4)) was proposed by  
304 Knutson and Whitby (1975) and they noted that sizing is crucially dependent on flow rates and high voltage  
305 (HV) applied to the DMA. In our study, the flow accuracy calibrated by the mass flow meter (TSI series  
306 4000) is within  $\pm 2\%$ . The variation of voltage applied to the nano-DMA (0-12500 V, 0-350 V) around the  
307 set value were measured with voltage power supply (HCE 0-12500, HCE 0-350, Fug Electronic) and  
308 summarized in Table S5. According to the error propagation formula (see SI. S2. Eq. (S5)) (Taylor and  
309 Taylor, 1997), the calculated uncertainty in sizing of 6-100 nm nanoparticles increases as size decreases  
310 (Table S5). The estimated sizing accuracy is slightly smaller than the sizing offset of two nano-DMA, but  
311 in principle they are still consistent with each other. This suggests that uncertainties of slip correction, DMA

312 dimensions (inner and outer radius, length), temperature, pressure, and viscosity of air may also affect the  
313 sizing accuracy (see SI. S2. Eq. (S4), Kinney et al., 1991). Besides, Wiedensohler et al. (2012) also  
314 suggested that particle losses, the size- and material-dependent CPC counting efficiency can affect the size  
315 accuracy of DMAs.

316 After calibration, on average a <1.4% sizing offset between the two nano-DMAs can be achieved for  
317 ammonium sulfate nanoparticles with dry diameters of 100 nm, 60 nm and 20 nm (Fig. 3c, Fig.5, Table S3,  
318 Fig. S4, and Fig. S5), which is much better than the 2-3% criteria recommended by Massling et al. (2011)  
319 and Zhang et al. (2016). For sub-10 nm ammonium sulfate nanoparticles, our system has an average sizing  
320 offset of <0.9% for 10 and 8 nm particles and ~1.4% for 6 nm particles, respectively (Fig. 3d, Fig. 5, Table  
321 S3, and Fig. S6). As discussed above, uncertainties in the sheath flow rates and nano-DMA voltages will  
322 increase as size decreases, which results in a larger sizing offset of 6-nm nanoparticles compared with other  
323 sizes. Note that, we also tested to calibrate the DMA voltage with a voltage meter with lower accuracy of  
324  $\pm 1\%$ , and the DMA voltages can only be kept within  $\pm 1\%$  around the set value. In this way, we found a  
325 much larger sizing offset for the sub-10 nm particles, i.e., 5.4% and 6.0% for 8 and 6 nm ammonium sulfate  
326 nanoparticles, respectively. These results show that maintaining an accurate sheath/aerosol flow (with  $\pm 1\%$   
327 around the set value) together with a careful voltage calibration (with  $\pm 0.1\%$  around the set value, especially  
328 in low voltage range, i.e., <50 V for our system) is the key for accurate sizing of sub-10 nm nanoparticles.

### 329 **3.1.2 Preventing pre-deliqescence in the deliqescence measurement mode**

330 Pre-deliqescence of dry nanoparticles in the deliqescence measurement mode is an important issue that  
331 needs to be resolved in order to obtain accurate DRH (Biskos et al., 2006b; Duplissy et al., 2009;  
332 Bezantakos et al., 2016; Hämeri et al., 2000). Since temperature and RH are closely linked and accurate  
333 monitoring of these two quantities in the system are critical for nano-HTDMA measurements, we calibrated  
334 all RH and T sensors regularly (every two weeks in this study). To prevent pre-deliqescence and optimize  
335 the system, we have conducted three tests using ammonium sulfate nanoparticles with a dry diameter of

100 nm. In the first test, we regulated the RH of excess flow ( $RH_e$ ) and made it equal to that of the aerosol flow at the inlet of nano-DMA2 ( $RH_a$ ), i.e.,  $RH_e = RH_a$ , as done by previous HTDMA measurements, e.g., Villani et al. (2008). As shown in Fig. 4a, the measured growth factors of 100-nm ammonium sulfate are in good agreement with predictions of the Extended Aerosol Inorganic Model (E-AIM; Clegg et al., 1998) at RH above 80%. However, the ammonium sulfate nanoparticles deliquesce at 75% RH, which is significantly lower than the expected DRH (80%, Tang and Munkelwitz (1994)). Since our RH sensors were all well calibrated and the uncertainty of RH measurement is  $\pm 1\%$ , it is reasonable to hypothesize that the RH upstream of nano-DMA2 has already reached the deliquesce RH of ammonium sulfate nanoparticles. When these aerosol nanoparticles move downstream of the nano-DMA2, the RH decreases back to 75%, which dehydrates the deliquesced ammonium sulfate nanoparticles. To avoid the pre-deliquescence, Hämeri et al. (2001) has suggested to set  $RH_a$  to be 3-5% lower than  $RH_e$ . In the second test, we have configured and regulated the system following this suggestion, i.e.,  $RH_e \geq RH_a + 3\%$ . In this case, the ammonium sulfate nanoparticles still deliquesce at 79% RH (Fig. 4b), even if  $RH_a$  is 6% lower than  $RH_e$ .

Previous studies (Biskos et al., 2006b; Bezantakos et al., 2016) have shown that RH non-uniformities within the nano-DMA2 can result in inaccurate measurements of phase transition and hygroscopic growth of aerosol nanoparticles. One reason for RH non-uniformities within nano-DMA2 is that the sheath flow RH is different from the aerosol flow RH at the inlet of the DMA (Hämeri et al., 2000, 2001). Another important reason is the existence of temperature gradient within nano-DMA2 (Bezantakos et al., 2016). Hence, in the third test, we moved the RH sensor from the excess flow downstream of nano-DMA2 to the sheath flow upstream of nano-DMA2 and then regulated RH of sheath flow ( $RH_s$ ) the same as  $RH_a$  (shown in Fig. 1), i.e.,  $RH_s = RH_a$ , as done by Kreidenweis et al. (2005), Biskos et al. (2006a, b), and Massling et al. (2011). Note that to minimize the temperature gradient within the nano-DMA2 in our system so that nanoparticles can undergo almost the same RH conditions, the nano-DMA2 with its sheath flow humidification system has been placed in a well-insulated air-conditioned chamber. The air temperature inside the chamber can

be maintained at an almost constant level ( $292.15 \pm 0.1$  K). In addition, a heat exchanger was installed downstream of the recirculation blower to minimize the temperature perturbation in the sheath flow by the heat generated in the RB. Unlike previously reported by Bezantakos et al. (2016) that the RH at the outlet was higher than that the inlet of the sheath air, we monitored that the sheath flow temperature at the inlet of nano-DMA2 is slightly lower (less than  $\sim 0.2$  K) than that at the outlet, i.e., the RH<sub>s</sub> at the inlet of nano-DMA2 is slightly higher ( $\sim 1\%$ ) than the RH of the excess air at the outlet. It may due to the heat produced from the inner electrode of nano-DMA2, which we estimated to be  $\sim 0.08$  W ( $Q = mdTC_{p,k}$ ) by considering the density and heating capacity of air, and aerosol and sheath air flow rate ( $\rho = 1.2041 \text{ kg/m}^3$ ;  $C_p = 1.859 \text{ kJ/kg}^\circ\text{C}$ ) (Atkins et al., 2006). Although this temperature perturbation (less than  $\sim 0.2$  K between the sheath flow at the inlet and the excess flow at the outlet of the nano-DMA2) is larger than the ideal condition of less than  $0.1$  K that Duplissy et al. (2009) and Wiedensohler et al. (2012) suggested, our experimental results show that a prompt phase transition can be still achieved. In this case, the measured DRH of ammonium sulfate nanoparticles is almost at  $80\%$  (Fig. 4c and 4d).

### 3.1.3 Prompt phase transition of ammonium sulfate

Figure 5 and 6 show the normalized particle number size distributions measured by the nano-DMA2 in the respective deliquescence and efflorescence measurement modes for ammonium sulfate nanoparticles with dry mobility diameters of  $20$  nm,  $10$  nm, and  $6$  nm (see Fig. S4 for  $100$  nm, see Fig. S5 for  $60$  nm, see Fig. S6 for  $8$  nm). In the deliquescence measurement mode (Fig. 5, Fig. S4a, and Fig. S5a), we observed the similar double-mode phenomenon as reported by Mikhailov et al. (2004) and Biskos et al. (2006b, 2007). For example, at  $20$  nm, there are two distinct intersecting modes of particle size distributions determined by the nano-DMA2 in the RH range from  $79\%$  to  $83\%$  RH (around the DRH of ammonium sulfate). Biskos et al. (2006b, 2007) attributed these two modes to the co-existence of solid and liquid phase nanoparticles at RH close to the DRH of ammonium sulfate, due to the slight inhomogeneity of RH in the second nano-DMA, i.e., some nanoparticles have already undergo deliquescence (liquid state) and some are not (solid).

385 This is evident through a double-mode log-normal fitting (red and blue modes in Fig. 5). Until RH ~82%,  
386 the peak diameter of the red mode at 82% RH is similar to that at 11% RH, indicating that these  
387 nanoparticles are still in a solid state. At 82% RH, a population of ammonium sulfate nanoparticles starts  
388 to deliquesce and exists in a distinct mode with significant larger peak diameter (blue mode), although  
389 majority of the nanoparticles remain solid (red mode). Further increase RH, the peak diameter of  
390 normalized number size distribution of the blue mode increases, indicating the continuous growth the  
391 nanoparticles after deliquescence. However, in our case the double-mode phenomenon was not observed  
392 for 8 and 6 nm ammonium sulfate nanoparticles (Fig. 5 and Fig. S6a). To have a better estimation of DRH  
393 when the double modes occurred, the peak diameter of the mode with larger number of nanoparticles was  
394 chosen for growth factor calculation (Biskos et al., 2006b, 2007). For example, for 20 nm ammonium  
395 sulfate nanoparticles, the peak diameters of normalized number size distribution of the red and blue modes  
396 are used to calculate growth factor at RH between 79% to 83%, respectively.

397 For the efflorescence measurement mode, we adopted the approach of Biskos et al. (2006b) and used the  
398 geometric standard deviation of number size distribution (sigma:  $\sigma$ ) to quantify the diversity of the sizes of  
399 nanoparticles. As shown in Fig. 6, Fig. S4b, Fig. S5b, and Fig. S6b, broadening of the normalized number  
400 size distributions measured with nano-DMA2 was only observed for 20-nm ammonium sulfate  
401 nanoparticles in the RH range from 33% to 30%. There, at RH higher than 33% or lower than 30%,  $\sigma$  stays  
402 stably at 1.072. However, clear increases of  $\sigma$  (1.078-1.087) were observed for RH between 33% and 30%.  
403 The normalized number size distributions in the RH range from 33% to 30% can be further resolved by  
404 double-mode fit with fixed  $\sigma$  of 1.072 (the red and the blue mode in Fig. 6 for 20 nm). The ammonium  
405 sulfate nanoparticles in the red mode at RH between 33% to 30% are in solid state because the peak diameter  
406 of red mode is similar as that at 11% RH. However, within this RH range, the peak diameter of the blue  
407 mode is significantly larger, indicating that these nanoparticles are still in liquid state. Further decreasing  
408 RH (lower than 30%), only one mode has been observed and the peak diameter of the normalized number  
409 size distribution almost unchanged as RH decreases (red mode in Fig. 6 for 20nm), which means that the

nanoparticles have been all in the solid state. Similar to the deliquescence measurement shown above and in Fig. 5, the co-existence of solid and aqueous phase nanoparticles at RH 30-33% is also very likely to stem from the slight heterogeneous RH in nano-DMA2 (Biskos et al., 2006b). To have a better estimation of ERH when the broadening phenomenon exists, the peak diameter of the mode with larger number of nanoparticles was used for growth factor calculation. After such data processing in both deliquescence and efflorescence modes, we obtained prompt deliquescence and efflorescence of 6 to 100 nm ammonium sulfate nanoparticles (more details in Section 3.1.4).

### 3.1.4 Size-dependent hygroscopicity of ammonium sulfate nanoparticles

Figure 7 shows the humidogram of ammonium sulfate nanoparticles measured by our nano-HTDMA system in the size (dry diameter) range of 6-100 nm. The detailed comparison between our results and Biskos et al. (2006b) during both deliquescence and efflorescence measurements are presented in Fig. 8a and b (also Fig. S7). In general, our results are in a good agreement with the measurement results of Biskos et al (2006) and the theoretical prediction by Cheng et al. (2015). First, there is a strong size dependence in the hygroscopic growth factor of ammonium sulfate nanoparticles, and smaller ammonium sulfate nanoparticles exhibit lower growth factor at a certain RH. For example, the difference of the growth factor between 6 and 100 nm nanoparticles is up to 0.28 at 80% RH (Fig. S8a). Second, there is, however, no significant size dependence in both DRH and ERH (Fig. S8b). For nanoparticles of different sizes (6-100 nm), the DRH and ERH of ammonium sulfate varies slightly from ~80-83% and ~30-34%, respectively. This variation of the DRH and ERH along the size is much smaller for ammonium sulfate nanoparticles than for sodium chloride (Biskos et al. 2006a, 2007).

Although our results in general agree well with Biskos et al. (2006b), the growth factors of 10, 8, and 6 nm ammonium sulfate nanoparticles that we measured at high RH (i.e., > ~70%) are slightly lower (~0.02 in growth factor) than that in Biskos et al. (2006b) in both deliquescence and efflorescence processes (Fig. 8b and Fig. S7). We calculated the uncertainties of growth factor of 10-nm ammonium sulfate from 80% to

90% RH for our system and Biskos et al. (2006b) system by  $\sqrt{\left(g_f \frac{\sqrt{2}\epsilon_{Dp}}{D_p}\right)^2 + \left(\epsilon_{RH} \frac{dg_f}{dRH}\right)^2}$  (Mochida  
 and Kawamura, (2004)). Here,  $\epsilon_{Dp}$ ,  $\epsilon_{RH}$ , and  $g_f$  are uncertainty of particle mobility diameter, uncertainty  
 of relative humidity, and growth factor with respect to RH, respectively. The average sizing offsets of our  
 system and Biskos et al. (2006b) for 10 nm ammonium sulfate are taken here as  $\frac{\epsilon_{Dp}}{D_p}$  (see Table 1). As shown  
 in the insert of Fig. 8b, the discrepancies between the two systems are still within measurement uncertainty.

In addition, compared to Biskos et al. (2006b), our results show a similar re-structuring in deliquescence  
 mode at RH between about 20% to 75% for 100, and 60 nm ammonium sulfate nanoparticles (Fig 8c).  
 However, different than in Biskos et al. (2006b), we do not find re-structuring for smaller ammonium  
 sulfate nanoparticles (20, 10, 8, and 6 nm) at RH below deliquescence point (Fig. 8c and Fig. 8d). There  
 seems to be continuous water adsorption and the adsorbed water layers (Romakkaniemi et al., 2001)  
 become significantly thicker when RH closer to the DRH (i.e,  $RH > 70\%$ ). For example, a slight increase  
 in hygroscopic growth factor of 6-nm ammonium sulfate nanoparticles is observed in the RH range from  
 65 to 79% RH before deliquescence. This is attributed to water adsorption onto the surfaces of these  
 nanoparticles. It seems that smaller nanoparticles have a stronger tendency of adsorbing water when  
 approaching the DRH than the larger ones. Similar phenomenon has also observed by Hämeri et al. (2000,  
 2001), Romakkaniemi et al. (2001), Biskos et al. (2006a, b, 2007), and Giamarelou et al. (2018). The reason  
 for such enhanced adsorption at smaller sizes is still to be investigated. Note that, the ammonium sulfate  
 hygroscopic data from Biskos et al. (2006b) shown here are all generated by an electrospray, but in our  
 experiments, only the ammonium sulfate nanoparticles with diameters smaller than 20 nm (i.e., 10, 8, and  
 6 nm) were generated by an electrospray, while the larger nanoparticles (i.e., 20, 60, and 100 nm) were  
 generated by a atomizer. Different from generation conditions of for 6-10 nm ammonium sulfate  
 nanoparticles in Biskos et al. (2006b), in our study, in order to minimize the multiple charged nanoparticles,  
 three different concentrations are used so that the size selected by the nano-DMA1 (i.e., 6, 8, 10 nm) was

always slight larger than peak of the number size distribution of the generated nanoparticles by the electrospray. This also helps us to have as many as nanoparticles as possible to compensate the strong nanoparticle losses in the nano-HTDMA system. In addition, we used both electrospray and atomizer to generate 20-nm ammonium sulfate, and compared their hygroscopic growth factors prior to deliquescence. Figure S12a shows a  $\sim 0.1$  higher growth factor of 20-nm ammonium sulfate generated by the electrospray than that using the atomizer in the RH range from 55% to 82%, which is similar to the difference in hygroscopic growth factor of 20-nm NaCl aerosol nanoparticles using the different generation method as observed in Fig S12b in Biskos et al. (2006a). Besides different generation conditions, the morphology of dried ammonium sulfate particles may also differ slightly between our study and Biskos et al. (2006) because of different drying rate, as drying flow rates and RH of the dried ammonium sulfate in the two HTDMA systems are different too. This means the different generation methods and drying conditions may influence the surface structure of the nanoparticles and thus their interaction with the adsorbed water layers (Iskandar et al., 2003; Xin et al., 2019).

### 3.2 Size-dependent hygroscopicity of sodium sulfate nanoparticles

As a common constituent of atmospheric aerosol particles (Tang and Munkelwitz, 1993, 1994; Tang 1996; Tang et al., 2007), hygroscopicity of sodium sulfate with diameters above 20 nm particles has been investigated by a few groups (Tang et al., 2007; Xu and Schweiger, 1999; Hu et al., 2010). However, its hygroscopic behavior in the sub-10 nm size range has not been investigated yet. In this study, we applied our nano-HTDMA system to measure the hygroscopic growth factors, DRH, and ERH of sodium sulfate nanoparticles with dry size from 20 nm down to 6 nm.

Figure 9 shows the measured size-resolved hygroscopic growth factors of sodium sulfate nanoparticles. Different from the observations by Tang et al. (2007) using an electrodynamic balance (EDB), we observed prompt deliquescence and efflorescence for both 20-nm and 6-nm sodium sulfate nanoparticles. Two intersecting modes in the measured number size distribution of humidified sodium sulfate nanoparticles are

481 observed at RH close to the DRH (Fig. S9 and S10 in the Supplementary Information) and ERH, suggesting  
482 an externally mixed of aqueous and solid nanoparticles. As shown in Sect. 3.1.3, a similar phenomenon is  
483 also observed for ammonium sulfate, which could be attributed to the slight RH heterogeneities in nano-  
484 DMA2, which makes only part of the nanoparticles deliquesce at RH close to the DRH, while the others  
485 remain in solid state.

486 Together with the hygroscopic growth of 14-16  $\mu\text{m}$  and 200-20 nm sodium sulfate measured previously by  
487 Tang et al. (2007) and Hu et al. (2010), we show a strong size dependence in hygroscopic growth factors  
488 of sodium sulfate nanoparticles (Fig. S11d). For example, at RH 84%, the hygroscopic growth factor of 6  
489 nm sodium sulfate is only  $\sim 1.3$  (in efflorescence mode), while the respective growth factors are about 1.5  
490 and 1.8 for 20 nm and 14-16  $\mu\text{m}$  particles. As shown in Fig. 9, E-AIM already agrees well with the  
491 hygroscopic growth of micrometer particles (14-16  $\mu\text{m}$ ) without shape correction (DeCarlo et al., 2004),  
492 i.e., shape factor ( $\chi$ ) of 1.0. However, to explain observation, a shape factor of  $\sim 1.16$  and 1.26 would be  
493 needed for 20 nm and 6 nm sodium sulfate nanoparticles, respectively.

494 There is no significant change in DRH between 14-16  $\mu\text{m}$  ( $\sim 84\%$ ) and 20 nm ( $\sim 84\%$ ) sodium sulfate  
495 particles (Fig. 9). This is consistent with Hu et al. (2010) where no change in DRH from 200 nm down to  
496 20 nm ( $\sim 82\%$ , see Table 1 from Hu et al. (2010)) was observed. However, a significant increase of DRH  
497 occurred when further decreasing particle diameters to 6 nm (DRH =  $\sim 90\%$ ). The size dependence of ERH  
498 is stronger than that of DRH, as there is already a clear increase of ERH from micrometer 14-16  $\mu\text{m}$  ( $\sim 57\%$ )  
499 to 20 nm ( $\sim 62\%$ ) sodium sulfate particles. When further reducing the particle diameters to 6 nm, an almost  
500 6% increase of DRH can be found, compared to the micrometer 14-16  $\mu\text{m}$  particles (i.e., ERH increases  
501 from 57 to 82%, respectively). Different from ammonium sulfate, of which DRH and ERH shows no  
502 significant size dependence, there is a strong size-dependence of DRH and ERH of sodium sulfate  
503 according to our observations down to 6 nm. The different size dependence of DRH and ERH between  
504 sodium chloride and ammonium sulfate have been theoretically studied and explained by Cheng et al.

(2015). The main reason is the different concentration dependence of solute activities and the different solute-liquid surface tension, e.g., the same change in solute molality leads to a larger change in the solute activity of sodium chloride than that of ammonium sulfate. The phase transition concentration (deliquescence and crystallization concentration) of ammonium sulfate is thus more sensitive to the size change compared to that of sodium chloride, leading to the almost unchanged DRH and ERH of ammonium sulfate nanoparticles (Cheng et al., 2015). For the size dependence of phase transition of sodium sulfate, a strong size effect on DRH and ERH is similar to that of sodium chloride but different from that of ammonium sulfate in the size range from 6 to 20 nm, suggesting that non-ideality of solution property is close to that of sodium chloride but weaker than that of ammonium sulfate. As different hydrates of sodium sulfate may exist during the deliquescence and efflorescence processes (Xu and Schweiger, 1999), to explain the underline mechanism of the size dependent hygroscopicity of sodium sulfate particles can be challenging.

517

#### 518 **4 Summary and Conclusion**

519 In this study, we presented our newly designed and self-assembled nano-HTDMA for measuring  
520 hygroscopicity of nanoparticles in the sub-10 nm diameter size range. We also introduced the  
521 comprehensive methods for system calibration and reported the performance of the system, focusing on the  
522 sizing accuracy and preventing pre-deliqescence in the deliquescence measurement mode. By comparing  
523 with previous studies on ammonium sulfate nanoparticles (Biskos et al., 2006b), we show that our system  
524 is capable of providing high quality data of the hygroscopic behavior of sub-10 nm nanoparticles. We then  
525 extended our measurements for sodium sulfate nanoparticles, of which size-dependent deliquescence and  
526 efflorescence have been clearly observed for nanoparticles down to 6 nm in size, with similar behavior as  
527 sodium chloride.

As we know, atmospheric aerosol particles consist of not only inorganic components, but also a vast number of organic components existing in the atmosphere. However, their physico-chemical properties are still not fully understood, especially when comes to the nano-scale and supersaturated concentration range. The nano-HTDMA system can be directly applicable to explore the size dependence of aerosol nanoparticles. Combing the multi-size measurements of hygroscopicity and the Differential Köhler Analyses (DKA, Cheng et al., 2015) in nano size range, we will be able characterize and parameterize the water activity and surface tension of different inorganic and organic systems. This will further help us to understand the formation and transformation of aerosol nanoparticles in the atmosphere and their interaction with water vapor.

#### **Data availability**

Readers who are interested in the data should contact Yafang Cheng ([yafang.cheng@mpic.de](mailto:yafang.cheng@mpic.de)).

#### **Acknowledgement**

This study was supported by the Max Planck Society (MPG) and Leibniz Society. T.L. acknowledges the support from China Scholarship Council (CSC). Y.C. would like to acknowledge the Minerva Program of MPG.

**Author contributions:** Y.C. and H.S. designed and led the study. N.M., T.T. and A. W. assembled the basic HTDMA system. Y.C., H.S. and T.L. modified and advanced the basic system into the nano-HTDMA for the purpose of measuring hygroscopic properties of aerosol nanoparticles in sub-10 nm size range at MPIC. T.L. performed the experiments. J.H., N.M. and X.W. supported the experiments. All co-authors discussed the results and commented on the manuscript. T.L. wrote the manuscript with input from all co-authors.

## 550    **Reference**

- 551    Andreae, M. O., Afchine, A., Albrecht, R., Holanda, B. A., Artaxo, P., Barbosa, H. M. J., Borrmann, S.,  
552    Cecchini, M. A., Costa, A., Dollner, M., Fütterer, D., Järvinen, E., Jurkat, T., Klimach, T., Konemann, T.,  
553    Knote, C., Krämer, M., Krisna, T., Machado, L. A. T., Mertes, S., Minikin, A., Pöhlker, C., Pöhlker, M. L.,  
554    Pöschl, U., Rosenfeld, D., Sauer, D., Schlager, H., Schnaiter, M., Schneider, J., Schulz, C., Spanu, A.,  
555    Sperling, V. B., Voigt, C., Walser, A., Wang, J., Weinzierl, B., Wendisch, M., and Ziereis, H.: Aerosol  
556    characteristics and particle production in the upper troposphere over the Amazon Basin, *Atmos. Chem.*  
557    *Phys.*, 18, 921-961, 2018.
- 558    Atkins, P., De Paula, J., and Walters, V.: *Physical Chemistry*, W. H. Freeman, 2006.
- 559    Badger, C. L., George, I., Griffiths, P. T., Braban, C. F., Cox, R. A., and Abbatt, J. P. D.: Phase transitions  
560    and hygroscopic growth of aerosol particles containing humic acid and mixtures of humic acid and  
561    ammonium sulphate, *Atmospheric Chemistry and Physics*, 6, 755-768, 2006.
- 562    Bezantakos, S., Huang, L., Barmounis, K., Martin, S. T., and Biskos, G.: Relative humidity non-  
563    uniformities in Hygroscopic Tandem Differential Mobility Analyzer measurements, *Journal of Aerosol*  
564    *Science*, 101, 1-9, 2016.
- 565    Birmili, W., Stratmann, F., Wiedensohler, A., Covert, D., M. Russell, L., and Berg, O.: Determination of  
566    Differential Mobility Analyzer Transfer Functions Using Identical Instruments in Series, 1997.
- 567    Birmili, W., Weinhold, K., Rasch, F., Sonntag, A., Sun, J., Merkel, M., Wiedensohler, A., Bastian, S.,  
568    Schladitz, A., Löschau, G., Cyrys, J., Pitz, M., Gu, J., Kusch, T., Flentje, H., Quass, U., Kaminski, H.,  
569    Kuhlbusch, T. A. J., Meinhardt, F., and Fiebig, M.: Long-term observations of tropospheric particle number  
570    size distributions and equivalent black carbon mass concentrations in the German Ultrafine Aerosol  
571    Network (GUAN), 2016.

572 Biskos, G., Malinowski, A., Russell, L. M., Buseck, P. R., and Martin, S. T.: Nanosize Effect on the  
 573 Deliquescence and the Efflorescence of Sodium Chloride Particles, *Aerosol Science and Technology*, 40,  
 574 97-106, 2006a.

575 Biskos, G., Paulsen, D., Russell, L. M., Buseck, P. R., and Martin, S. T.: Prompt deliquescence and  
 576 efflorescence of aerosol nanoparticles, *Atmospheric Chemistry and Physics*, 6, 4633-4642, 2006b.

577 Biskos, G., Russell, L. M., Buseck, P. R., and Martin, S. T.: Nanosize effect on the hygroscopic growth  
 578 factor of aerosol particles, *Geophysical Research Letters*, 33, 2007.

579 Chan, M. N. and Chan, C. K.: Hygroscopic properties of two model humic-like substances and their  
 580 mixtures with inorganics of atmospheric importance, *Environmental Science & Technology*, 37, 5109-  
 581 5115, 2003.

582 Chan, M. N. and Chan, C. K.: Mass transfer effects in hygroscopic measurements of aerosol particles,  
 583 *Atmospheric Chemistry and Physics*, 2005.

584 Chan, M. N., Kreidenweis, S. M., and Chan, C. K.: Measurements of the Hygroscopic and Deliquescence  
 585 Properties of Organic Compounds of Different Solubilities in Water and Their Relationship with Cloud  
 586 Condensation Nuclei Activities, *Environmental Science & Technology*, 42, 3602-3608, 2008.

587 Chen, Da-Ren, David Y.H. Pui, and Stanley L. Kaufman.: Electrospinning of conducting liquids for  
 588 monodisperse aerosol generation in the 4 nm to 1.8  $\mu\text{m}$  diameter range, *J. Aerosol Sci.*, 26: 963-977, 1995.

589 Cheng, Y., Su, H., Koop, T., Mikhailov, E., and Pöschl, U.: Size dependence of phase transitions in aerosol  
 590 nanoparticles, *Nature communications*, 6, 5923, 2015.

591 Cheng, Y., Zheng, G., Wei, C., Mu, Q., Zheng, B., Wang, Z., Gao, M., Zhang, Q., He, K., Carmichael, G.,  
 592 Pöschl, U., and Su, H.: Reactive nitrogen chemistry in aerosol water as a source of sulfate during haze  
 593 events in China, *Science Advances*, 2, e1601530, 2016.

594 Cheng, Y. F., Berghof, M., Garland, R. M., Wiedensohler, A., Wehner, B., Muller, T., Su, H., Zhang, Y.  
 595 H., Achtert, P., Nowak, A., Poschl, U., Zhu, T., Hu, M., and Zeng, L. M.: Influence of soot mixing state on  
 596 aerosol light absorption and single scattering albedo during air mass aging at a polluted regional site in  
 597 northeastern China, *Journal of Geophysical Research-Atmospheres*, 114, 2009.

598 Cheng, Y. F., Wiedensohler, A., Eichler, H., Heintzenberg, J., Tesche, M., Ansmann, A., Wendisch, M.,  
 599 Su, H., Althausen, D., Herrmann, H., Gnauk, T., Brüggemann, E., Hu, M., and Zhang, Y. H.: Relative  
 600 humidity dependence of aerosol optical properties and direct radiative forcing in the surface boundary layer  
 601 at Xinken in Pearl River Delta of China: An observation based numerical study, *Atmospheric Environment*,  
 602 42, 6373-6397, 2008.

603 Clegg, S. L., Brimblecombe, P., and Wexler, A. S.: Thermodynamic Model of the System  $\text{H}^+ - \text{NH}_4^+ - \text{SO}_4^{2-}$   
 604  $- \text{NO}_3^- - \text{H}_2\text{O}$  at Tropospheric Temperatures, *The Journal of Physical Chemistry A*, 102, 2137-2154, 1998.

605 Collins, D. R., Cocker, D. R., Flagan, R. C., and Seinfeld, J. H.: The Scanning DMA Transfer Function,  
 606 *Aerosol Science and Technology*, 38, 833-850, 2004.

607 Cruz, C. N. and Pandis, S. N.: Deliquescence and Hygroscopic Growth of Mixed Inorganic–Organic  
 608 Atmospheric Aerosol, *Environmental Science & Technology*, 34, 4313-4319, 2000.

609 DeCarlo, P. F., Slowik, J. G., Worsnop, D. R., Davidovits, P., and Jimenez, J. L.: Particle Morphology and  
 610 Density Characterization by Combined Mobility and Aerodynamic Diameter Measurements. Part 1:  
 611 Theory, *Aerosol Science and Technology*, 38, 1185-1205, 2004.

612 Dong, J. L., Xiao, H. S., Zhao, L. J., and Zhang, Y.-H.: Spatially resolved Raman investigation on phase  
 613 separations of mixed  $\text{Na}_2\text{SO}_4/\text{MgSO}_4$  droplets, 2009.

614 Dougle, P. G., Veefkind, J. P., and ten Brink, H. M.: Crystallisation of mixtures of ammonium nitrate,  
 615 ammonium sulphate and soot, *Journal of Aerosol Science*, 29, 375-386, 1998.

616 Dunne, E. M., Gordon, H., Kürten, A., Almeida, J., Duplissy, J., Williamson, C., Ortega, I. K., Pringle, K.  
 617 J., Adamov, A., Baltensperger, U., Barmet, P., Benduhn, F., Bianchi, F., Breitenlechner, M., Clarke, A.,  
 618 Curtius, J., Dommen, J., Donahue, N. M., Ehrhart, S., Flagan, R. C., Franchin, A., Guida, R., Hakala, J.,  
 619 Hansel, A., Heinritzi, M., Jokinen, T., Kangasluoma, J., Kirkby, J., Kulmala, M., Kupc, A., Lawler, M. J.,  
 620 Lehtipalo, K., Makhmutov, V., Mann, G., Mathot, S., Merikanto, J., Miettinen, P., Nenes, A., Onnela, A.,  
 621 Rap, A., Reddington, C. L. S., Riccobono, F., Richards, N. A. D., Rissanen, M. P., Rondo, L., Sarnela, N.,  
 622 Schobesberger, S., Sengupta, K., Simon, M., Sipilä, M., Smith, J. N., Stozkhov, Y., Tomé, A., Tröstl, J.,  
 623 Wagner, P. E., Wimmer, D., Winkler, P. M., Worsnop, D. R., and Carslaw, K. S.: Global atmospheric  
 624 particle formation from CERN CLOUD measurements, *Science*, 354, 1119-1124, 2016.

625 Duplissy, J., Gysel, M., S, S., Meyer, N., N, G., L, K., V, M., R, W., Martins dos Santos, S., C, G., Villani,  
 626 P., P, L., Sellegri, K., A, M., B. McFiggans, G., G, W., R, R., Dommen, J., Ristovski, Z., and Weingartner,  
 627 E.: Intercomparison study of six HTDMAs: results and general recommendations for HTDMA operation,  
 628 *Atmospheric Measurement Techniques*, 2. Pp, 363-378, 2009.

629 Ehn, M., Thornton, J. A., Kleist, E., Sipilä, M., Junninen, H., Pullinen, I., Springer, M., Rubach, F.,  
 630 Tillmann, R., Lee, B., Lopez-Hilfiker, F., Andres, S., Acir, I.-H., Rissanen, M., Jokinen, T., Schobesberger,  
 631 S., Kangasluoma, J., Kontkanen, J., Nieminen, T., Kurtén, T., Nielsen, L. B., Jørgensen, S., Kjaergaard, H.  
 632 G., Canagaratna, M., Maso, M. D., Berndt, T., Petäjä, T., Wahner, A., Kerminen, V.-M., Kulmala, M.,  
 633 Worsnop, D. R., Wildt, J., and Mentel, T. F.: A large source of low-volatility secondary organic aerosol,  
 634 *Nature*, 506, 476, 2014.

635 Eichler, H., Cheng, Y., Birmili, W., Nowak, A., Wiedensohler, A., Brüggemann, E., Gnauk, T., Herrmann,  
 636 H., Althausen, D., Ansmann, A., Engelmann, R., Tesche, M., Wendisch, M., Zhang, Y. H., Hu, M., Liu, S.,  
 637 and Zeng, L.: Hygroscopic properties and extinction of aerosol particles at ambient relative humidity in  
 638 South-Eastern China, 2008.

639 Estillore, A. D., Morris, H. S., Or, V. W., Lee, H. D., Alves, M. R., Marciano, M. A., Laskina, O., Qin, Z.,  
 640 Tivanski, A. V., and Grassian, V. H.: Linking hygroscopicity and the surface microstructure of model  
 641 inorganic salts, simple and complex carbohydrates, and authentic sea spray aerosol particles, *Physical*  
 642 *Chemistry Chemical Physics*, 19, 21101-21111, 2017.

643 Fan, J., Rosenfeld, D., Zhang, Y., Giangrande, S. E., Li, Z., Machado, L. A. T., Martin, S. T., Yang, Y.,  
 644 Wang, J., Artaxo, P., Barbosa, H. M. J., Braga, R. C., Comstock, J. M., Feng, Z., Gao, W., Gomes, H. B.,  
 645 Mei, F., Pöhlker, C., Pöhlker, M. L., Pöschl, U., and de Souza, R. A. F.: Substantial convection and  
 646 precipitation enhancements by ultrafine aerosol particles, *Science*, 359, 411-418, 2018.

647 Gao, Y., Chen, S. B., and Yu, L. E.: Efflorescence Relative Humidity for Ammonium Sulfate Particles,  
 648 *The Journal of Physical Chemistry A*, 110, 7602-7608, 2006.

649 Ghorai, S., Wang, B., Tivanski, A., and Laskin, A.: Hygroscopic Properties of Internally Mixed Particles  
 650 Composed of NaCl and Water-Soluble Organic Acids, *Environmental Science & Technology*, 48, 2234-  
 651 2241, 2014.

652 Giamarelou, M., Smith, M., Papapanagiotou, E., Martin, S. T., and Biskos, G.: Hygroscopic properties of  
 653 potassium-halide nanoparticles, *Aerosol Science and Technology*, 52, 536-545, 2018.

654 Gysel, M., Weingartner, E., and Baltensperger, U.: Hygroscopicity of aerosol particles at low temperatures.  
 655 2. Theoretical and experimental hygroscopic properties of laboratory generated aerosols, *Environmental*  
 656 *Science & Technology*, 36, 63-68, 2002.

657 Hämeri, K., Laaksonen, A., Väkevä, M., and Suni, T.: Hygroscopic growth of ultrafine sodium chloride  
 658 particles, *Journal of Geophysical Research: Atmospheres*, 106, 20749-20757, 2001.

659 Hämeri, K., Väkevä, M., Hansson, H.-C., and Laaksonen, A.: Hygroscopic growth of ultrafine ammonium  
 660 sulfate aerosol measured using an ultrafine tandem differential mobility analyzer, *Journal of Geophysical*  
 661 *Research: Atmospheres*, 105, 22231-22242, 2000.

662 Hansson, H.-C., Rood, M. J., Koloutsou-Vakakis, S., Hämeri, K., Orsini, D., and Wiedensohler, A.: NaCl  
 663 Aerosol Particle Hygroscopicity Dependence on Mixing with Organic Compounds, *Journal of Atmospheric*  
 664 *Chemistry*, 31, 321-346, 1998.

665 Hennig, T., Massling, A., Brechtel, F. J., and Wiedensohler, A.: A tandem DMA for highly temperature-  
 666 stabilized hygroscopic particle growth measurements between 90 % and 98% relative humidity, *Journal of*  
 667 *Aerosol Science*, 36, 1210-1223, 2005.

668 Hong, J., Häkkinen, S. A. K., Paramonov, M., Äijälä, M., Hakala, J., Nieminen, T., Mikkilä, J., Prisle, N.  
 669 L., Kulmala, M., Riipinen, I., Bilde, M., Kerminen, V. M., and Petäjä, T.: Hygroscopicity, CCN and  
 670 volatility properties of submicron atmospheric aerosol in a boreal forest environment during the summer  
 671 of 2010, *Atmos. Chem. Phys.*, 14, 4733-4748, 2014.

672 Hong, J., Kim, J., Nieminen, T., Duplissy, J., Ehn, M., Äijälä, M., Hao, L. Q., Nie, W., Sarnela, N., Prisle,  
 673 N. L., Kulmala, M., Virtanen, A., Petäjä, T., and Kerminen, V. M.: Relating the hygroscopic properties of  
 674 submicron aerosol to both gas- and particle-phase chemical composition in a boreal forest environment,  
 675 *Atmos. Chem. Phys.*, 15, 11999-12009, 2015.

676 Hu, D., Qiao, L., Chen, J.-M., Ye, X., Yang, X., Cheng, T., and Fang, W.: Hygroscopicity of Inorganic  
 677 Aerosols: Size and Relative Humidity Effects on the Growth Factor, 2010.

678 Iskandar, F., Gradon, L., and Okuyama, K.: Control of the morphology of nanostructured particles prepared  
 679 by the spray drying of a nanoparticle sol, *Journal of Colloid and Interface Science.*, 265, 296-303, 2003.

680 Kerminen, V. M.: The effects of particle chemical character and atmospheric processes on particle  
 681 hygroscopic properties, *Journal of Aerosol Science*, 28, 121-132, 1997.

682 Keskinen, H., Virtanen, A., Joutsensaari, J., Tsagkogeorgas, G., Duplissy, J., Schobesberger, S., Gysel, M.,  
 683 Riccobono, F., Slowik, J. G., Bianchi, F., Yli-Juuti, T., Lehtipalo, K., Rondo, L., Breitenlechner, M., Kupc,  
 684 A., Almeida, J., Amorim, A., Dunne, E. M., Downard, A. J., Ehrhart, S., Franchin, A., Kajos, M. K., Kirkby,  
 685 J., Kürten, A., Nieminen, T., Makhmutov, V., Mathot, S., Miettinen, P., Onnela, A., Petäjä, T., Praplan, A.,  
 686 Santos, F. D., Schallhart, S., Sipilä, M., Stozhkov, Y., Tomé, A., Vaattovaara, P., Wimmer, D., Prevot, A.,  
 687 Dommen, J., Donahue, N. M., Flagan, R. C., Weingartner, E., Viisanen, Y., Riipinen, I., Hansel, A.,  
 688 Curtius, J., Kulmala, M., Worsnop, D. R., Baltensperger, U., Wex, H., Stratmann, F., and Laaksonen, A.:  
 689 Evolution of particle composition in CLOUD nucleation experiments, *Atmos. Chem. Phys.*, 13, 5587-5600,  
 690 2013.

691 Kim, J., Ahlm, L., Yli-Juuti, T., Lawler, M., Keskinen, H., Tröstl, J., Schobesberger, S., Duplissy, J.,  
 692 Amorim, A., Bianchi, F., Donahue, N. M., Flagan, R. C., Hakala, J., Heinritzi, M., Jokinen, T., Kürten, A.,  
 693 Laaksonen, A., Lehtipalo, K., Miettinen, P., Petäjä, T., Rissanen, M. P., Rondo, L., Sengupta, K., Simon,  
 694 M., Tomé, A., Williamson, C., Wimmer, D., Winkler, P. M., Ehrhart, S., Ye, P., Kirkby, J., Curtius, J.,  
 695 Baltensperger, U., Kulmala, M., Lehtinen, K. E. J., Smith, J. N., Riipinen, I., and Virtanen, A.:  
 696 Hygroscopicity of nanoparticles produced from homogeneous nucleation in the CLOUD experiments,  
 697 *Atmos. Chem. Phys.*, 16, 293-304, 2016.

698 Kinney, P. D., Pui, D. Y. H., Mullholland, G. W. & Bryner, N. P. Use of the Electrostatic Classification  
 699 Method to Size 0.1  $\mu\text{m}$  SRM Particles—A Feasibility Study. *Journal of Research of the National Institute*  
 700 *of Standards and Technology.*, 96, 147, 1991.

701 Kirkby, J., Curtius, J., Almeida, J., Dunne, E., Duplissy, J., Ehrhart, S., Franchin, A., Gagné, S., Ickes, L.,  
 702 Kürten, A., Kupc, A., Metzger, A., Riccobono, F., Rondo, L., Schobesberger, S., Tsagkogeorgas, G.,  
 703 Wimmer, D., Amorim, A., Bianchi, F., Breitenlechner, M., David, A., Dommen, J., Downard, A., Ehn, M.,

704 Flagan, R. C., Haider, S., Hansel, A., Hauser, D., Jud, W., Junninen, H., Kreissl, F., Kvashin, A.,  
 705 Laaksonen, A., Lehtipalo, K., Lima, J., Lovejoy, E. R., Makhmutov, V., Mathot, S., Mikkilä, J., Minginette,  
 706 P., Mogo, S., Nieminen, T., Onnela, A., Pereira, P., Petäjä, T., Schnitzhofer, R., Seinfeld, J. H., Sipilä, M.,  
 707 Stozhkov, Y., Stratmann, F., Tomé, A., Vanhanen, J., Viisanen, Y., Vrtala, A., Wagner, P. E., Walther, H.,  
 708 Weingartner, E., Wex, H., Winkler, P. M., Carslaw, K. S., Worsnop, D. R., Baltensperger, U., and Kulmala,  
 709 M.: Role of sulphuric acid, ammonia and galactic cosmic rays in atmospheric aerosol nucleation, *Nature*,  
 710 476, 429-433, 2011.

711 Knutson, E. O. and Whitby, K. T.: Aerosol classification by electric mobility: apparatus, theory, and  
 712 applications, *Journal of Aerosol Science*, 6, 443-451, 1975.

713 Köhler, H.: The nucleus in and the growth of hygroscopic droplets, *Transactions of the Faraday Society*,  
 714 32, 1152-1161, 1936.

715 Kreidenweis, S. M., Koehler, K., DeMott, P. J., Prenni, A. J., Carrico, C., and Ervens, B.: Water activity  
 716 and activation diameters from hygroscopicity data - Part I: Theory and application to inorganic salts,  
 717 *Atmospheric Chemistry and Physics*, 5, 1357-1370, 2005.

718 Lei, T., Zuend, A., Cheng, Y., Su, H., Wang, W., and Ge, M.: Hygroscopicity of organic surrogate  
 719 compounds from biomass burning and their effect on the efflorescence of ammonium sulfate in mixed  
 720 aerosol particles, *Atmos. Chem. Phys.*, 18, 1045-1064, 2018.

721 Lei, T., Zuend, A., Wang, W. G., Zhang, Y. H., and Ge, M. F.: Hygroscopicity of organic compounds from  
 722 biomass burning and their influence on the water uptake of mixed organic ammonium sulfate aerosols,  
 723 *Atmos. Chem. Phys.*, 14, 11165-11183, 2014.

724 Lihavainen, H., Kerminen, V.-M., Komppula, M., Hatakka, J., Aaltonen, V., Kulmala, M., and Viisanen,  
 725 Y.: Production of “potential” cloud condensation nuclei associated with atmospheric new-particle  
 726 formation in northern Finland, *Journal of Geophysical Research: Atmospheres*, 108, 2003.

727 Martin, S. T.: Phase Transitions of Aqueous Atmospheric Particles, *Chemical Reviews*, 100, 3403-3454,  
 728 2000.

729 Massling, A., Niedermeier, N., Hennig, T., Fors, E. O., Swietlicki, E., Ehn, M., Hämeri, K., Villani, P., Laj,  
 730 P., Good, N., McFiggans, G., and Wiedensohler, A.: Results and recommendations from an  
 731 intercomparison of six Hygroscopicity-TDMA systems, *Atmos. Meas. Tech.*, 4, 485-497, 2011.

732 McMurry, P. H.: A review of atmospheric aerosol measurements, *Atmospheric Environment*, 34, 1959-  
 733 1999, 2000.

734 Mikhailov, E., Vlasenko, S., Martin, S. T., Koop, T., and Poschl, U.: Amorphous and crystalline aerosol  
 735 particles interacting with water vapor: conceptual framework and experimental evidence for restructuring,  
 736 phase transitions and kinetic limitations, *Atmospheric Chemistry and Physics*, 9, 9491-9522, 2009.

737 Mikhailov, E., Vlasenko, S., Niessner, R., and Poschl, U.: Interaction of aerosol particles composed of  
 738 protein and salts with water vapor: hygroscopic growth and microstructural rearrangement, *Atmospheric*  
 739 *Chemistry and Physics*, 4, 323-350, 2004.

740 Mikhailov, E., Vlasenko, S., Rose, D., and Pöschl, U.: Mass-based hygroscopicity parameter interaction  
 741 model and measurement of atmospheric aerosol water uptake, *Atmos. Chem. Phys.*, 13, 717-740, 2013.

742 Mikhailov, E. F. and Vlasenko, S. S.: High humidity tandem differential mobility analyzer for accurate  
 743 determination of aerosol hygroscopic growth, microstructure and activity coefficients over a wide range of  
 744 relative humidity, *Atmos. Meas. Tech. Discuss.*, <https://doi.org/10.5194/amt-2019-478>, in review, 2019.

745 Mikhailov, E. F., Vlasenko, S. S., and Ryshkevich, T. I.: Influence of chemical composition and  
 746 microstructure on the hygroscopic growth of pyrogenic aerosol, *Izvestiya, Atmospheric and Oceanic*  
 747 *Physics*, 44, 416-431, 2008.

748 Mirabel, P., Reiss, H., and Bowles, R. K.: A theory for the deliquescence of small particles, The Journal of  
 749 Chemical Physics, 113, 8200-8205, 2000.

750 Mochida, M. and Kawamura, K.: Hygroscopic properties of levoglucosan and related organic compounds  
 751 characteristic to biomass burning aerosol particles, Journal of Geophysical Research-Atmospheres, 109,  
 752 2004.

753 Mulholland, G. W., Donnelly, M. K., Hagwood, C. R., Kukuck, S. R., Hackley, V. A., and Pui, D. Y. H.:  
 754 Measurement of 100 nm and 60 nm Particle Standards by Differential Mobility Analysis, Journal of  
 755 Research of the National Institute of Standards and Technology, 111, 257-312, 2006.

756 Park, K., Kim, J.-S., and Miller, A. L.: A study on effects of size and structure on hygroscopicity of  
 757 nanoparticles using a tandem differential mobility analyzer and TEM, Journal of Nanoparticle Research,  
 758 11, 175-183, 2009.

759 Peng, C., Chow, A. H. L., and Chan, C. K.: Hygroscopic Study of Glucose, Citric Acid, and Sorbitol Using  
 760 an Electrodynamic Balance: Comparison with UNIFAC Predictions, Aerosol Science and Technology, 35,  
 761 753-758, 2001.

762 Pope, F. D., Dennis-Smith, B. J., Griffiths, P. T., Clegg, S. L., and Cox, R. A.: Studies of Single Aerosol  
 763 Particles Containing Malonic Acid, Glutaric Acid, and Their Mixtures with Sodium Chloride. I.  
 764 Hygroscopic Growth, The Journal of Physical Chemistry A, 114, 5335-5341, 2010.

765 Pruppacher, H. R. & Klett, J. D: Microphysics of clouds and precipitation, Kluwer Academic Publishers,  
 766 1997.

767 Rader, D. J. and McMurry, P. H.: Application of the tandem differential mobility analyzer to studies of  
 768 droplet growth or evaporation, Journal of Aerosol Science, 17, 771-787, 1986.

769 Raoux, S., Rettner, C. T., Jordan-Sweet, J. L., Kellock, A. J., Topuria, T., Rice, P. M., and Miller, D. C.:  
 770 Direct observation of amorphous to crystalline phase transitions in nanoparticle arrays of phase change  
 771 materials, *Journal of Applied Physics*, 102, 094305, 2007.

772 Reid, J. P., Dennis-Smith, B. J., Kwamena, N.-O. A., Miles, R. E. H., Hanford, K. L., and Homer, C. J.:  
 773 The morphology of aerosol particles consisting of hydrophobic and hydrophilic phases: hydrocarbons,  
 774 alcohols and fatty acids as the hydrophobic component, *Physical Chemistry Chemical Physics*, 13, 15559-  
 775 15572, 2011.

776 Richardson, C. B. and Spann, J.: Measurement of Water Cycle in a Levitated Ammonium Sulfate Particles,  
 777 1984.

778 Rickards, A. M. J., Miles, R. E. H., Davies, J. F., Marshall, F. H., and Reid, J. P.: Measurements of the  
 779 Sensitivity of Aerosol Hygroscopicity and the  $\kappa$  Parameter to the O/C Ratio, *The Journal of Physical*  
 780 *Chemistry A*, 117, 14120-14131, 2013.

781 Romakkaniemi, S., Hämeri, K., Väkevä, M., and Laaksonen, A.: Adsorption of Water on 8–15 nm NaCl  
 782 and (NH<sub>4</sub>)<sub>2</sub>SO<sub>4</sub> Aerosols Measured Using an Ultrafine Tandem Differential Mobility Analyzer, *The*  
 783 *Journal of Physical Chemistry A*, 105, 8183-8188, 2001.

784 Russell, L. M. and Ming, Y.: Deliquescence of small particles, *Journal of Chemical Physics*, 116, 311-321,  
 785 2002.

786 Sakurai, H., A. Fink, M., H. McMurry, P., Mauldin, R., F. Moore, K., N. Smith, J., and Eisele, F.:  
 787 Hygroscopicity and volatility of 4–10 nm particles during summertime atmospheric nucleation events in  
 788 urban Atlanta, 2005.

789 Seinfeld, J. H., and S. N. Pandis: *Atmospheric Chemistry and Physics: From Air Pollution to Climate*  
 790 *Change*, 2nd ed., John Wiley, New York, 2006.

791 Sihto, S. L., Mikkilä, J., Vanhanen, J., Ehn, M., Liao, L., Lehtipalo, K., Aalto, P. P., Duplissy, J., Petäjä,  
792 T., Kerminen, V. M., Boy, M., and Kulmala, M.: Seasonal variation of CCN concentrations and aerosol  
793 activation properties in boreal forest, *Atmos. Chem. Phys.*, 11, 13269-13285, 2011.

794 Stock, M., Cheng, Y. F., Birmili, W., Massling, A., Wehner, B., Müller, T., Leinert, S., Kalivitis, N.,  
795 Mihalopoulos, N., and Wiedensohler, A.: Hygroscopic properties of atmospheric aerosol particles over the  
796 Eastern Mediterranean: implications for regional direct radiative forcing under clean and polluted  
797 conditions, *Atmos. Chem. Phys.*, 11, 4251-4271, 2011.

798 Su, H., Rose, D., Cheng, Y. F., Gunthe, S. S., Massling, A., Stock, M., Wiedensohler, A., Andreae, M. O.,  
799 and Pöschl, U.: Hygroscopicity distribution concept for measurement data analysis and modeling of aerosol  
800 particle mixing state with regard to hygroscopic growth and CCN activation, *Atmos. Chem. Phys.*, 10,  
801 7489-7503, 2010.

802 Tang, I. N.: Chemical and size effects of hygroscopic aerosols on light scattering coefficients, *Journal of*  
803 *Geophysical Research: Atmospheres*, 101, 19245-19250, 1996.

804 Tang, I. N., Fung, K. H., Imre, D. G., and Munkelwitz, H. R.: Phase Transformation and Metastability of  
805 Hygroscopic Microparticles, *Aerosol Science and Technology*, 23, 443-453, 2007.

806 Tang, I. N. and Munkelwitz, H. R.: Composition and temperature dependence of the deliquescence  
807 properties of hygroscopic aerosols, *Atmospheric Environment. Part A. General Topics*, 27, 467-473, 1993.

808 Tang, I. N. and Munkelwitz, H. R.: Water activities, densities, and refractive indices of aqueous sulfates  
809 and sodium nitrate droplets of atmospheric importance, *Journal of Geophysical Research: Atmospheres*,  
810 99, 18801-18808, 1994.

811 Tang, M., Chan, C. K., Li, Y. J., Su, H., Ma, Q., Wu, Z., Zhang, G., Wang, Z., Ge, M., Hu, M., He, H., and  
812 Wang, X.: A review of experimental techniques for aerosol hygroscopicity studies, *Atmos. Chem. Phys.*,  
813 19, 12631-12686, 2019.

814 Topping, D., McFiggans, G., and Coe, H.: A curved multi-component aerosol hygroscopicity model  
815 framework: Part 1–Inorganic compounds, *Atmospheric Chemistry and Physics*, 5, 1205-1222, 2005.

816 Taylor, J. R. and Taylor, S. L. L. J. R.: *Introduction To Error Analysis: The Study of Uncertainties in*  
817 *Physical Measurements*, University Science Books, 1997.

818 Villani, P., Picard, D., Michaud, V., Laj, P., and Wiedensohler, A.: Design and Validation of a Volatility  
819 Hygroscopic Tandem Differential Mobility Analyzer (VH-TDMA) to Characterize the Relationships  
820 Between the Thermal and Hygroscopic Properties of Atmospheric Aerosol Particles, *Aerosol Science and*  
821 *Technology*, 42, 729-741, 2008.

822 Vlasenko, S. S., Su, H., Pöschl, U., Andreae, M. O., and Mikhailov, E. F.: Tandem configuration of  
823 differential mobility and centrifugal particle mass analysers for investigating aerosol hygroscopic  
824 properties, *Atmos. Meas. Tech.*, 10, 1269-1280, 2017.

825 Wang, J., Krejci, R., Giangrande, S., Kuang, C., Barbosa, H. M. J., Brito, J., Carbone, S., Chi, X.,  
826 Comstock, J., Ditas, F., Lavric, J., Manninen, H. E., Mei, F., Moran-Zuloaga, D., Pöhlker, C., Pöhlker, M.  
827 L., Saturno, J., Schmid, B., Souza, R. A. F., Springston, S. R., Tomlinson, J. M., Toto, T., Walter, D.,  
828 Wimmer, D., Smith, J. N., Kulmala, M., Machado, L. A. T., Artaxo, P., Andreae, M. O., Petäjä, T., and  
829 Martin, S. T.: Amazon boundary layer aerosol concentration sustained by vertical transport during rainfall,  
830 *Nature*, 539, 416, 2016.

831 Wang, L., Khalizov, A. F., Zheng, J., Xu, W., Ma, Y., Lal, V., and Zhang, R.: Atmospheric nanoparticles  
832 formed from heterogeneous reactions of organics, *Nature Geoscience*, 3, 238, 2010.

833 Wang, X., Ma, N., Lei, T., Größ, J., Li, G., Liu, F., Meusel, H., Mikhailov, E., Wiedensohler, A., and Su,  
834 H.: Effective density and hygroscopicity of protein particles generated with spray-drying process, *Journal*  
835 *of Aerosol Science*, 137, 105441, 2019.

836 Wang, Z., Su, H., Wang, X., Ma, N., Wiedensohler, A., Pöschl, U., and Cheng, Y.: Scanning  
837 supersaturation condensation particle counter applied as a nano-CCN counter for size-resolved analysis of  
838 the hygroscopicity and chemical composition of nanoparticles, *Atmos. Meas. Tech.*, 8, 2161-2172,  
839 <https://doi.org/10.5194/amt-8-2161-2015>, 2015.

840 Wiedensohler, A., Birmili, W., Nowak, A., Sonntag, A., Weinhold, K., Merkel, M., Wehner, B., Tuch, T.,  
841 Pfeifer, S., Fiebig, M., Fjåraa, A. M., Asmi, E., Sellegri, K., Depuy, R., Venzac, H., Villani, P., Laj, P.,  
842 Aalto, P., Ogren, J. A., Swietlicki, E., Williams, P., Roldin, P., Quincey, P., Hüglin, C., Fierz-  
843 Schmidhauser, R., Gysel, M., Weingartner, E., Riccobono, F., Santos, S., Gruning, C., Faloon, K.,  
844 Beddows, D., Harrison, R., Monahan, C., Jennings, S. G., O'Dowd, C. D., Marinoni, A., Horn, H. G., Keck,  
845 L., Jiang, J., Scheckman, J., McMurry, P. H., Deng, Z., Zhao, C. S., Moerman, M., Henzing, B., de Leeuw,  
846 G., Löschau, G., and Bastian, S.: Mobility particle size spectrometers: harmonization of technical standards  
847 and data structure to facilitate high quality long-term observations of atmospheric particle number size  
848 distributions, *Atmos. Meas. Tech.*, 5, 657-685, 2012.

849 Wiedensohler, A., Cheng, Y. F., Nowak, A., Wehner, B., Achtert, P., Berghof, M., Birmili, W., Wu, Z. J.,  
850 Hu, M., Zhu, T., Takegawa, N., Kita, K., Kondo, Y., Lou, S. R., Hofzumahaus, A., Holland, F., Wahner,  
851 A., Gunthe, S. S., Rose, D., Su, H., and Pöschl, U.: Rapid aerosol particle growth and increase of cloud  
852 condensation nucleus activity by secondary aerosol formation and condensation: A case study for regional  
853 air pollution in northeastern China, *Journal of Geophysical Research: Atmospheres*, 114, 2009.

854 Wiedensohler, A., Wiesner, A., Weinhold, K., Birmili, W., Hermann, M., Merkel, M., Müller, T., Pfeifer,  
855 S., Schmidt, A., Tuch, T., Velarde, F., Quincey, P., Seeger, S., and Nowak, A.: Mobility particle size  
856 spectrometers: Calibration procedures and measurement uncertainties, *Aerosol Science and Technology*,  
857 52, 146-164, 2018.

858 Wise, M. E., Surratt, J. D., Curtis, D. B., Shilling, J. E., and Tolbert, M. A.: Hygroscopic growth of  
859 ammonium sulfate/dicarboxylic acids, *Journal of Geophysical Research-Atmospheres*, 108, 2003.

860 Wu, Z. J., Nowak, A., Poulain, L., Herrmann, H., and Wiedensohler, A.: Hygroscopic behavior of  
 861 atmospherically relevant water-soluble carboxylic salts and their influence on the water uptake of  
 862 ammonium sulfate, *Atmos. Chem. Phys.*, 11, 12617-12626, 2011.

863 Xu, B. and Schweiger, G.: In-situ Raman observation of phase transformation of Na<sub>2</sub>SO<sub>4</sub> during the  
 864 hydration/dehydration cycles on single levitated microparticle, 1999.

865 You, Y., Renbaum-Wolff, L., and Bertram, A. K.: Liquid–liquid phase separation in particles containing  
 866 organics mixed with ammonium sulfate, ammonium bisulfate, ammonium nitrate or sodium chloride,  
 867 *Atmos. Chem. Phys.*, 13, 11723-11734, 2013.

868 Zawadowicz, M. A., Proud, S. R., Seppäläinen, S. S., and Cziczo, D. J.: Hygroscopic and phase separation  
 869 properties of ammonium sulfate/organics/water ternary solutions, *Atmos. Chem. Phys.*, 15, 8975-8986,  
 870 2015.

871 Zhang, S. L., Ma, N., Kecorius, S., Wang, P. C., Hu, M., Wang, Z. B., Größ, J., Wu, Z. J., and Wiedensohler,  
 872 A.: Mixing state of atmospheric particles over the North China Plain, *Atmospheric Environment*, 125, 152-  
 873 164, 2016.

874 Zhao, L.-J., Zhang, Y.-H., Wei, Z.-F., Cheng, H., and Li, X.-H.: Magnesium Sulfate Aerosols Studied by  
 875 FTIR Spectroscopy: Hygroscopic Properties, Supersaturated Structures, and Implications for Seawater  
 876 Aerosols, *The Journal of Physical Chemistry A*, 110, 951-958, 2006.

877 Zheng, G. J., Duan, F. K., Su, H., Ma, Y. L., Cheng, Y., Zheng, B., Zhang, Q., Huang, T., Kimoto, T.,  
 878 Chang, D., Pöschl, U., Cheng, Y. F., and He, K. B.: Exploring the severe winter haze in Beijing: the impact  
 879 of synoptic weather, regional transport and heterogeneous reactions, *Atmos. Chem. Phys.*, 15, 2969-2983,  
 880 2015.

881

882 **Tables**883 **Table 1.** Accuracy, precision and sources of uncertainty associated with HTDMA measurements.

	Biskos et al. (2006b)	Hämeri et al. (2000)	Nano-HTDMA (This study)
<i>DMA System</i>			
Type of DMA1 & DMA2	TSI nano-DMAs	Hauke-type DMAs	Vienna-type short DMAs
Accuracy of aerosol flow in DMA2	±1% (0.3-1.5 l/min)	-	±1% (1.5 l/min)
Accuracy of sheath flow in DMA2	±1% (5-15 l/min)	-	±1% (10 l/min)
Accuracy of DMA voltage	±0.1% (0-500V)	-	±0.1% (0-350V)
Sizing accuracy of DMA2 using PSL	3%	-	0.4% (100-nm PSL)
Sizing agreement between DMAs	3.1% (10 nm) <sup>a</sup>	±1% <sup>b</sup>	0.6% (100 nm) <sup>c</sup>
using ammonium sulfate			0.5% (60 nm) <sup>c</sup>
			1.4% (20 nm) <sup>c</sup>
			0.9% (10 nm) <sup>c</sup>
			-0.2% (8 nm) <sup>c</sup>
			1.4% (6 nm) <sup>c</sup>
Precision of particle-sizing	<2%	-	<2% (6-200 nm) <sup>d</sup>

<b>Humidification System</b>			
Type of RH sensor	RH sensors (Omega Model HX93AV)	Dew point mirror (GE) RH sensors (Vaisala Humitter model 50Y)	Dew point mirror (Edge) RH sensors (Vaisala model HMT 330)
Accuracy of RH sensors (0-90% RH)	$\pm 2.5\%$ RH	$\pm 3\%$ RH <sup>e</sup>	$\pm 1\%$ (RH sensor)
Position of the probe in the system	Inlet of DMA2 (RH <sub>a</sub> sensor <sup>f</sup> , RH <sub>s</sub> sensor <sup>g</sup> )	Inlet of DMA2 (RH <sub>a</sub> sensor) & excess air (RH <sub>s</sub> sensor, dew point mirror)	Inlet of DMA2 (RH <sub>a</sub> sensor, RH <sub>s</sub> sensor) & excess air (dew point mirror)
RH setting	RH <sub>a</sub> =RH <sub>s</sub>	RH <sub>s</sub> $\geq$ RH <sub>a</sub> +3%	RH <sub>a</sub> =RH <sub>s</sub>
<b>Temperature Control System</b>			
Temperature control type	Thermally isolated environment (humidification+DMA2) <sup>h</sup>	Thermally isolated environment (DMA2)	Box T regulated (humidification+DMA2)
Difference in T between inlet and outlet of DMA2	-	-	<0.2°C

884 <sup>a</sup>Not reported.

885 <sup>a</sup> According to the scans of the second DMA for the hygroscopic growth of 10 nm ammonium sulfate and the growth factors at different RHs provided by Biskos et al.  
886 (2006b), we retrieved an average sizing offset of Biskos et al. (2006b) system to be ~3.1% at 10 nm (see SI, S1).

887 <sup>b</sup> Size range not given.

888 <sup>c</sup> See Table S2 in supporting information.

889 <sup>d</sup> Value calculated according to the relative standard derivation.

890 <sup>e</sup> From Vaisala Humitter model 50Y manual.

891 <sup>f</sup> RH<sub>a</sub>: the RH of aerosol flow.

892 <sup>g</sup> RH<sub>s</sub>: the RH of sheath flow.

893 <sup>h</sup> Bezantakos et al. (2016).

# Figures

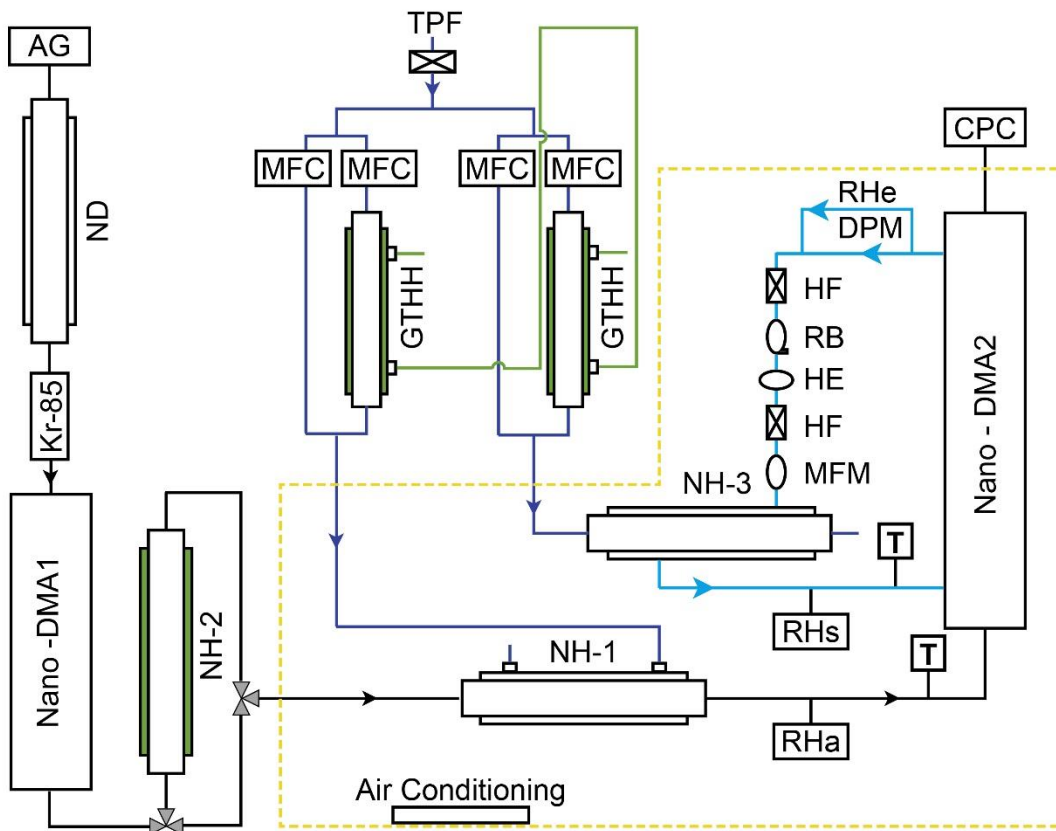


**Figure 1.** Experimental setup of the nano-HTDMA. Here, AG: aerosol generator (aerosol atomizer or electrospray); ND: nafen dryer; Kr-85: Krypton source aerosol neutralizer; Nano-DMA: nano differential mobility analyzer; TPF: total particle filter; HF: hydrophobic filter; MFC: mass flow controller; MFM: mass flow meter; RB: recirculation blower; DPM: dew point mirror; GTHH: Gore-Tex humidifier and heater; NH: nafen humidifier; HE: heat exchanger; CPC: condensation particle counter; Black line: aerosol line; Blue line: sheath line; Royal blue line: humidified air; Green line: MilliQ water (resistivity of 18.2 MΩ cm at 298.15 K). RH<sub>a</sub> and RH<sub>s</sub> (measured by RH sensors) represent the RH of aerosol and sheath flow in the inlet of nano-DMA2, respectively. RH<sub>e</sub> (measured by dew point) represents the RH of excess air. T represent the temperature of aerosol and sheath flow in the inlet of nano-DMA2, respectively.

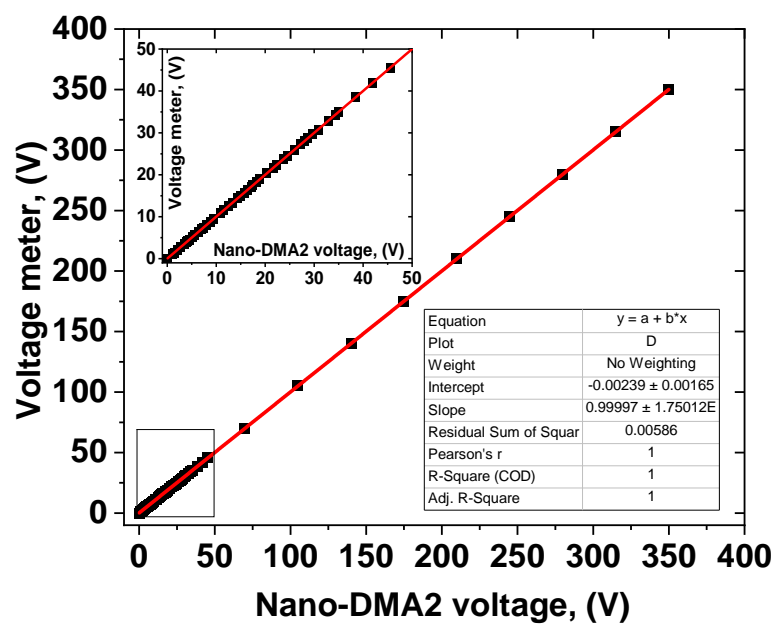


**Figure 2.** An example of voltage calibration of the nano-DMA2.

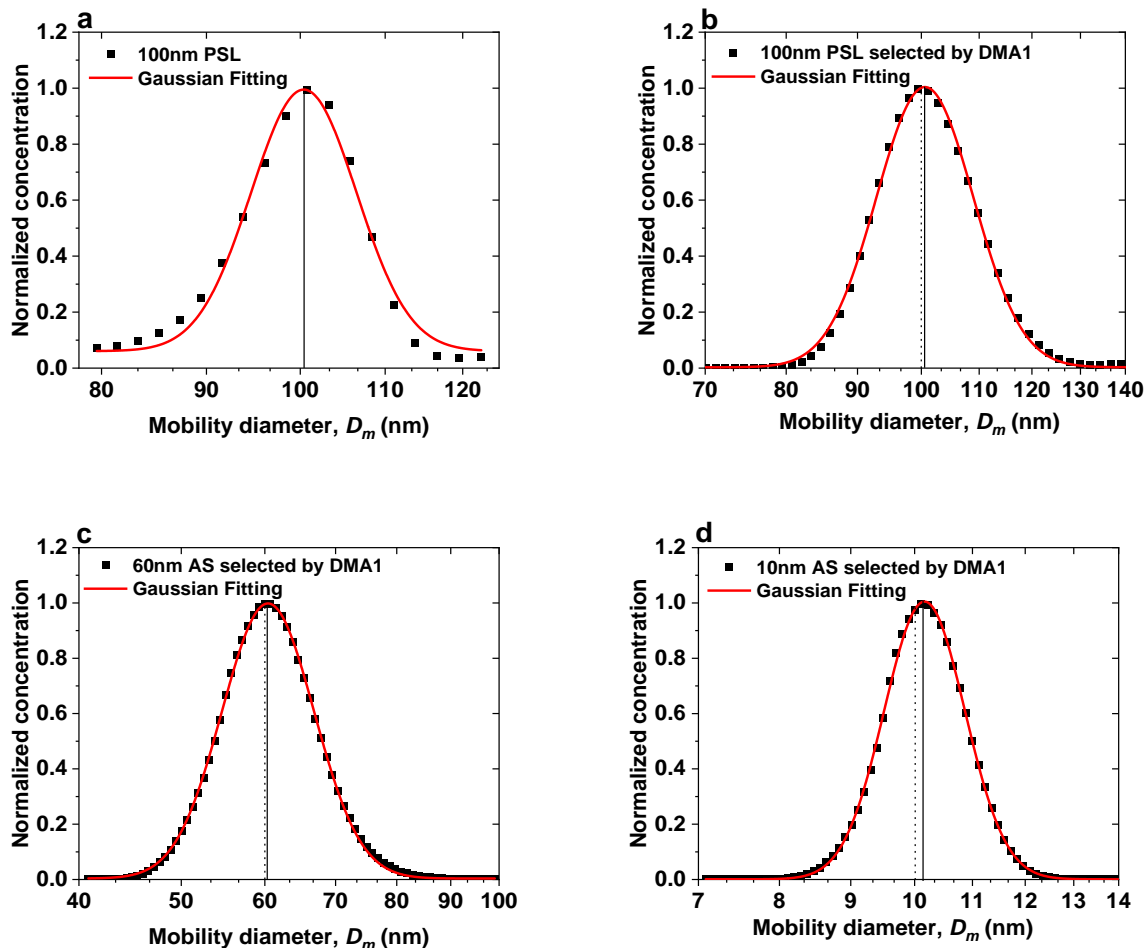


**Figure 3.** Sizing accuracy and sizing offset of nano-DMAs after calibration. **(a)** Normalized number size distribution scanned by the nano-DMA2 for 100-nm PSL nanoparticles (black solid square). The black solid line marks peak diameter from the Gaussian fits for the scan (red curve). Normalized number size distributions scanned by the nano-DMA2 for 100-nm PSL nanoparticles **(b)**, 60-nm **(c)**, and 10-nm **(d)** ammonium sulfate (AS) selected by the nano-DMA1 at RH below 5% at 298 K (black solid square). The dotted lines mark the diameters of the monodispersed nanoparticles selected by the nano-DMA1, i.e., 100 nm in **(b)**, 60 nm in **(c)** and 10 nm in **(d)**. The black solid lines mark the peak diameters from the Gaussian fits (red curve).

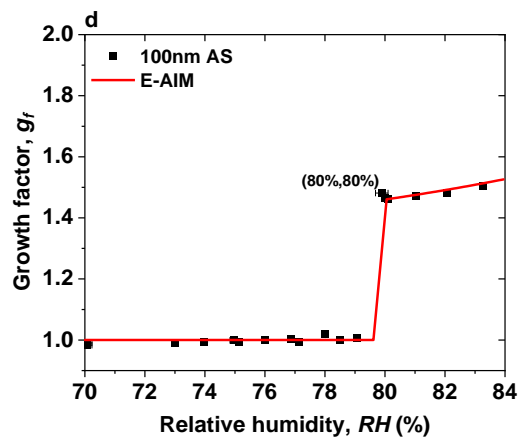
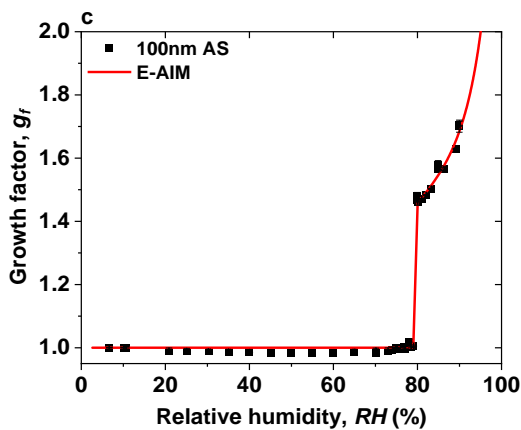
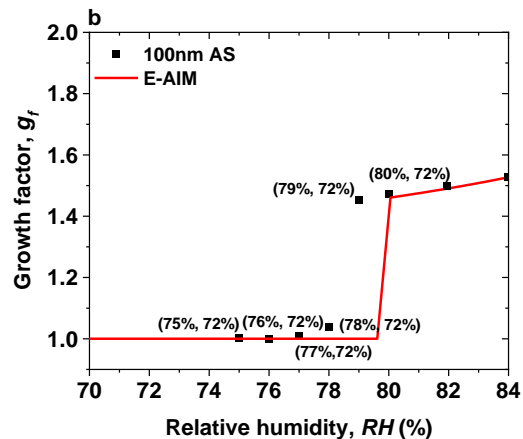
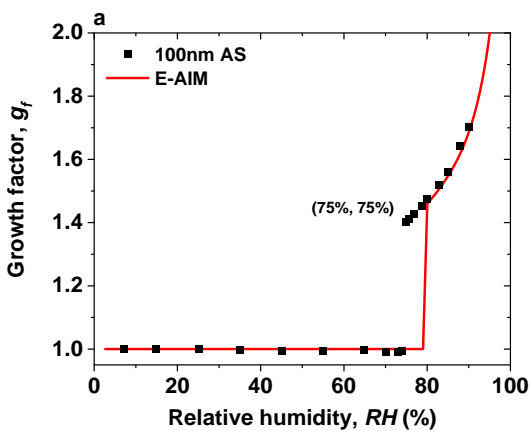


**Figure 4.** Mobility-diameter hygroscopic growth factors ( $g_f$ ) of 100-nm ammonium sulfate (AS) nanoparticles at 298 K measured in deliquescence mode. In comparison, the E-AIM model predicted growth factors of ammonium sulfate nanoparticles at 100 nm. (a)  $RH_e = RH_a$ , (75%, 75%) represents the ( $RH_e$ ,  $RH_a$ ), (b)  $RH_e \geq RH_a + 3\%$ , (75%, 72%) represents the ( $RH_e$ ,  $RH_a$ ), and (c)  $RH_s = RH_a$ . (d) The enlarged view of the RH range of 70% to 84% in Fig. 4c. (80%, 80%) represents the ( $RH_s$ ,  $RH_a$ ).  $RH_s$  and  $RH_e$  are the RH of sheath flow in the inlet of nano-DMA2 and in the excess air line, respectively;  $RH_a$  is the RH of aerosol flow in the inlet of nano-DMA2.

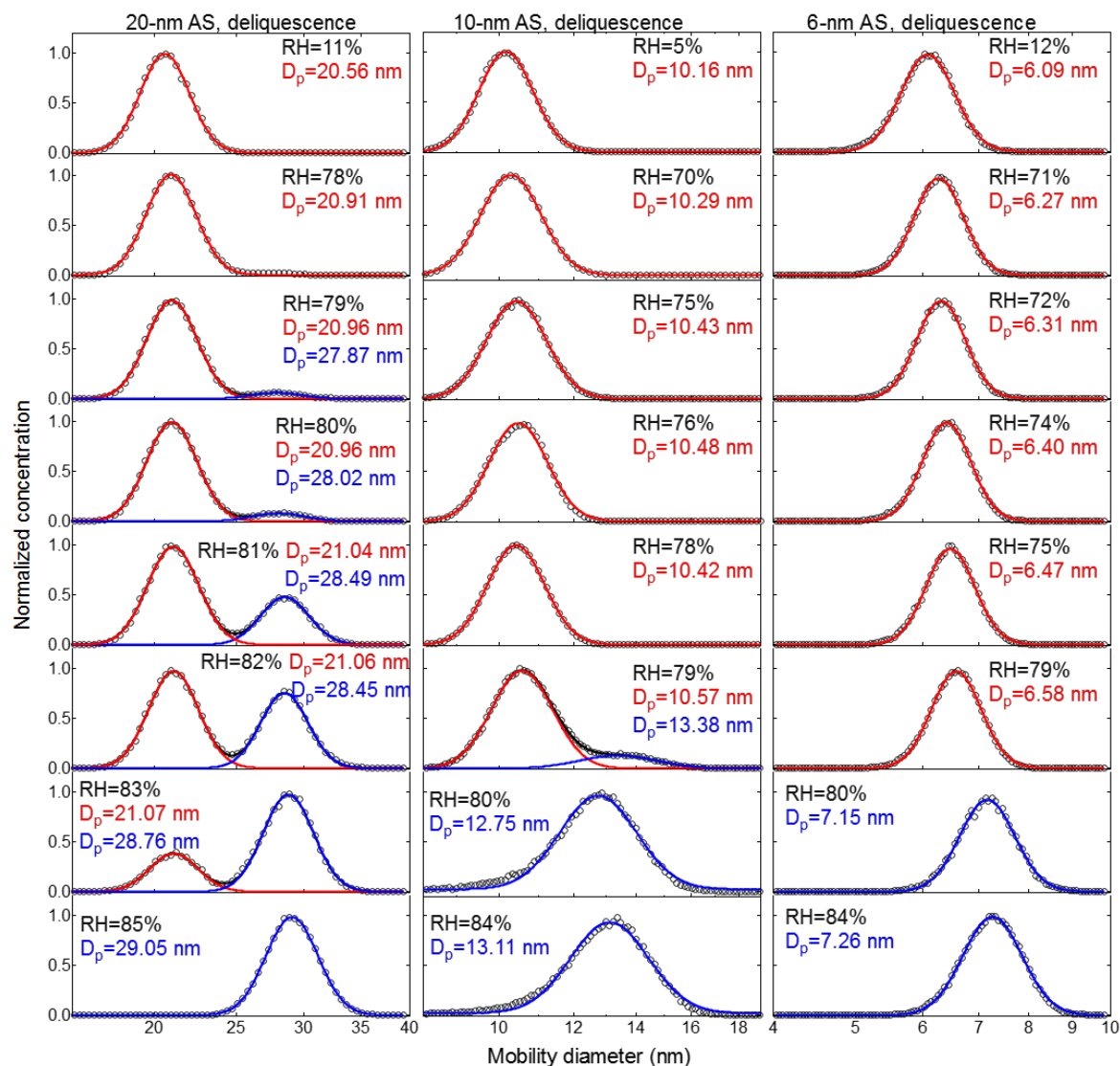


**Figure 5.** Deliquescence-mode measurements of ammonium sulfate (AS) aerosol nanoparticles with dry mobility diameter from 20-6nm. The measured (black square) and fitted (solid lines) normalized size distribution are shown for increasing RH. The red and blue lines represent the aerosol nanoparticles in the solid and liquid state, respectively. The RH history in each measurement is 5%  $\rightarrow$  X%, where X is the RH value given in each panel.

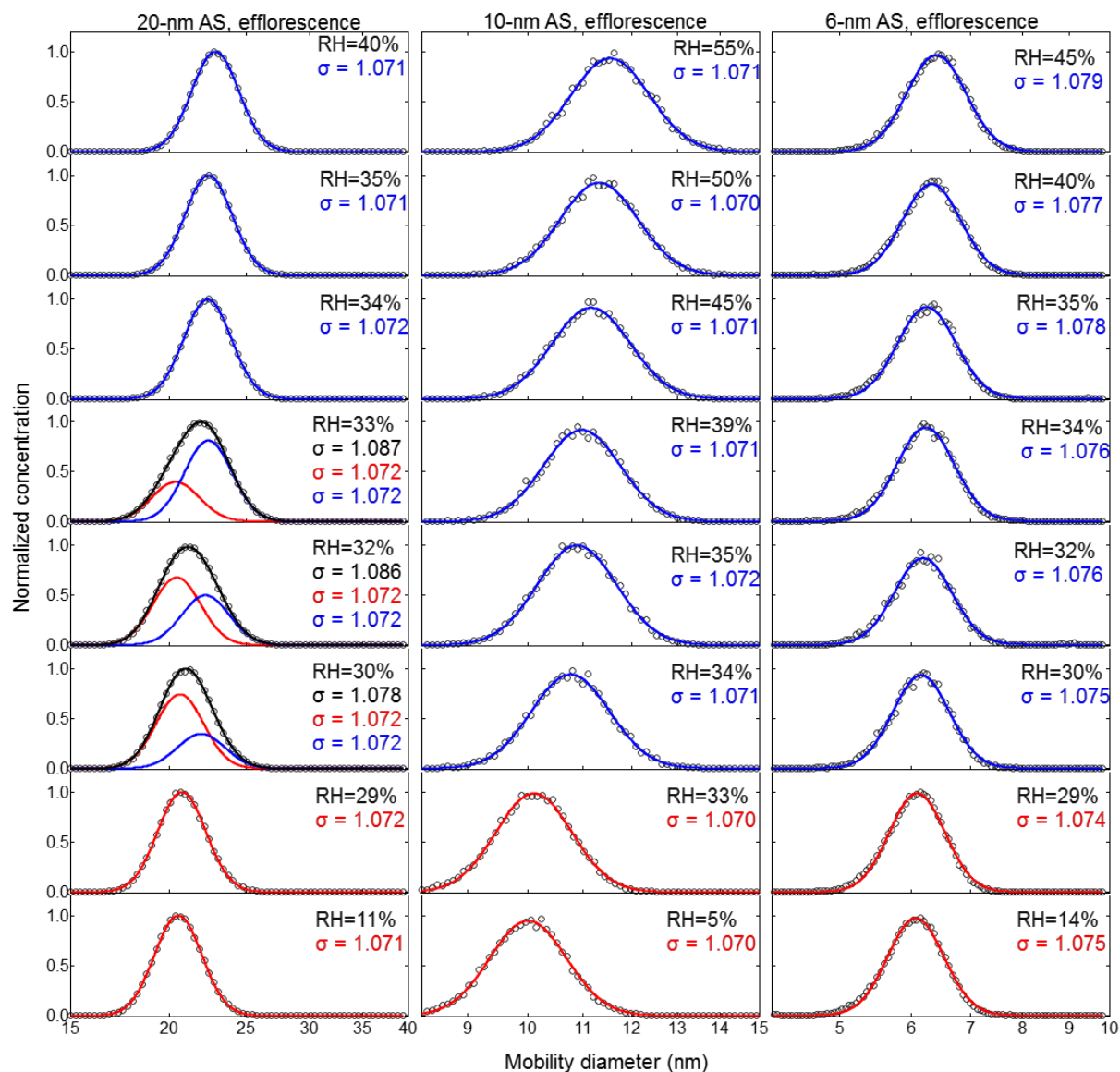


**Figure 6.** Efflorescence-mode measurements of ammonium sulfate (AS) aerosol nanoparticles with dry mobility diameter from 20-6nm. The measured (black circle) and fitted (solid lines) normalized size distribution are shown for increasing RH. The red and blue lines represent the aerosol nanoparticles in the solid and liquid state, respectively. The RH history in each measurement is 5%→97%→X%, where X is the RH value given in each panel.

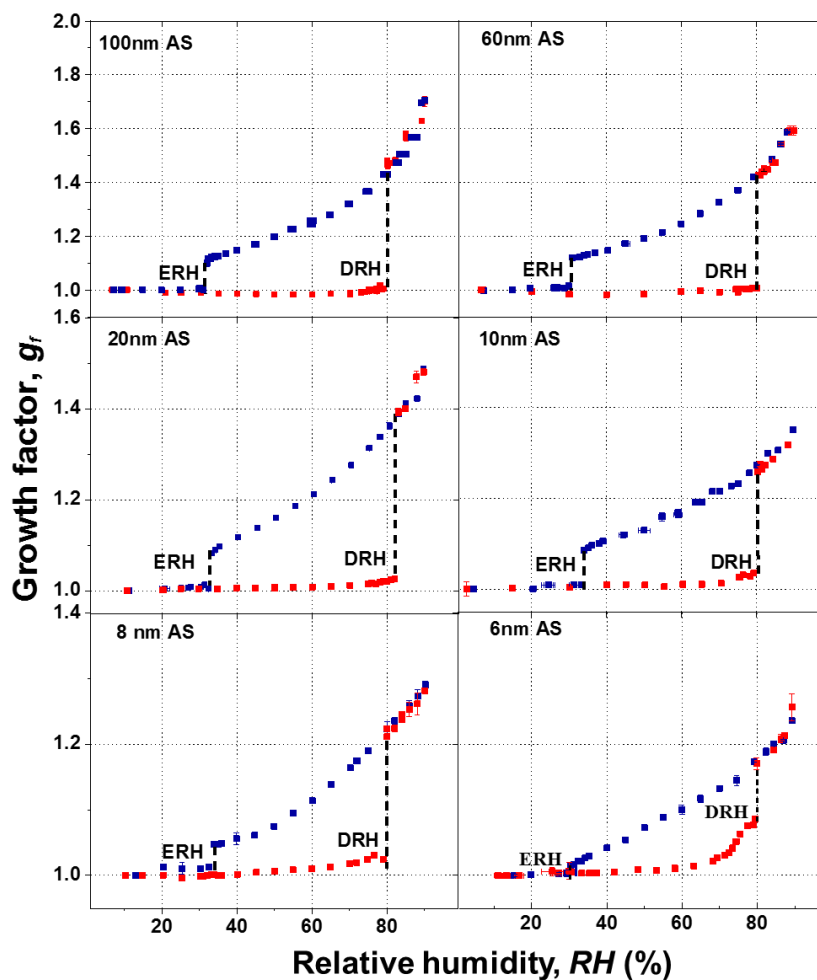


**Figure 7.** Mobility-diameter hygroscopic growth factors ( $g_r$ ) of ammonium sulfate (AS) aerosol nanoparticles with dry mobility diameter from 6 to 100 nm in the deliquescence mode (red square and error bar) and the efflorescence mode (blue square and error bar). Deliquescence, and efflorescence relative humidity (DRH&ERH, black dashed line) of ammonium sulfate (AS) nanoparticles with dry mobility diameter from 6 to 100 nm.

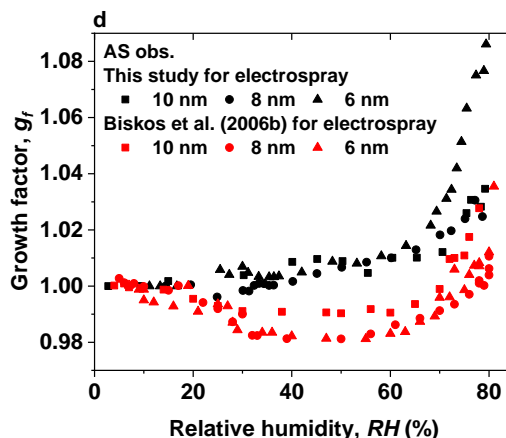
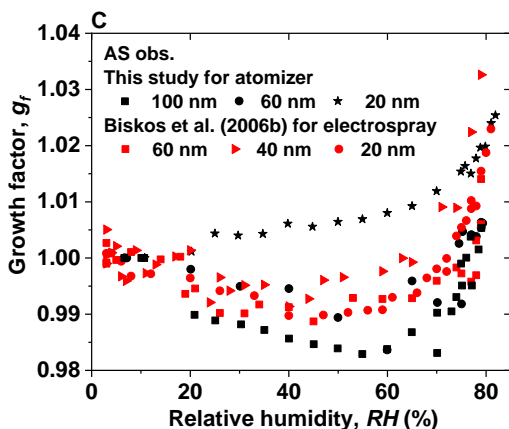
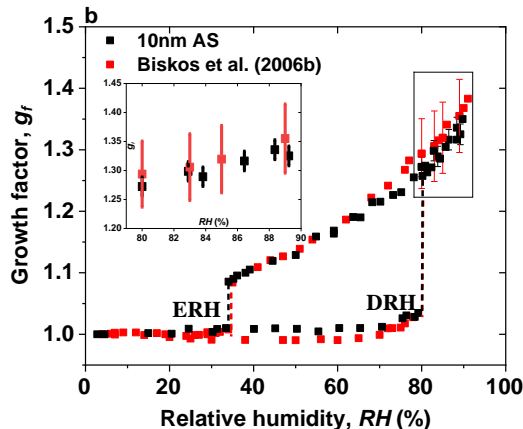
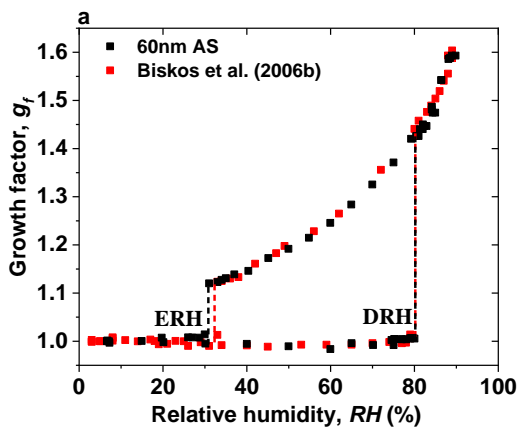


**Figure 8.** (a-b) Mobility-diameter hygroscopic growth factors ( $g_f$ , black squares), deliquescence and efflorescence relative humidity (DRH&ERH, black dashed lines) of ammonium sulfate (AS) nanoparticles with dry diameter 60 and 10 nm, respectively. Red squares and dashed lines show the respective results from Biskos et al. (2006b), respectively.

Black and red uncertainties of growth factors at certain RH are calculated by  $\sqrt{\left(\left(g_f \frac{\sqrt{2}\epsilon_{Dp}}{D_p}\right)^2 + \left(\epsilon_{RH} \frac{dg_f}{dRH}\right)^2\right)}$ , where  $\epsilon_{Dp}$ ,  $\epsilon_{RH}$ , and  $g_f$  are uncertainty of particle mobility diameter, uncertainty of relative humidity, and growth factor with respect to RH, respectively (Mochida and Kawamura 2004). (c-d) Comparison of growth factors of ammonium sulfate (AS) nanoparticles with dry diameter range from 6 to 100 nm with Biskos et al. (2006b) prior to deliquescence of ammonium sulfate nanoparticles.

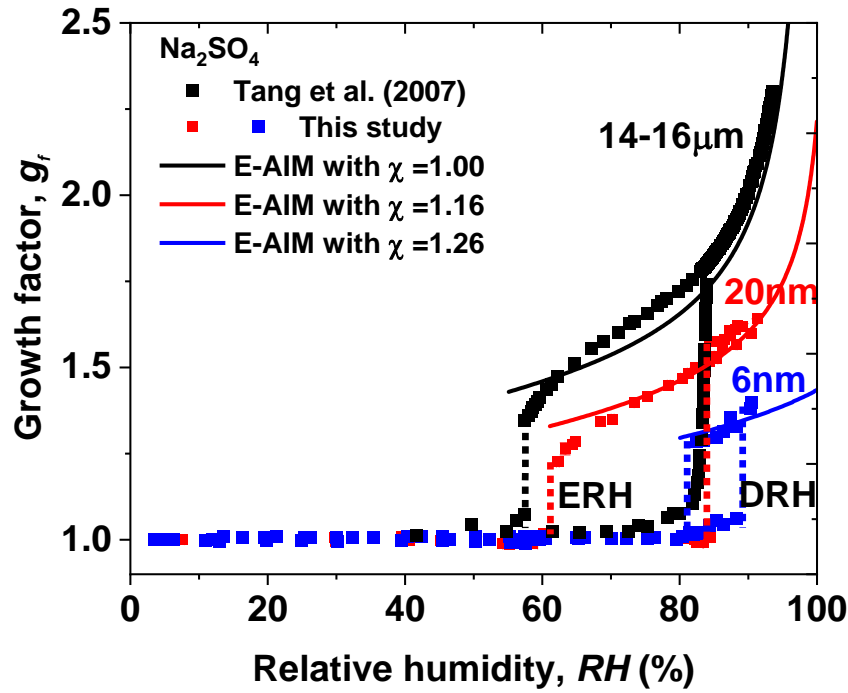


**Figure 9.** Mobility-diameter hygroscopic growth factors ( $g_r$ ), deliquescence and efflorescence relative humidity (DRH&ERH, red and blue dashed lines) of sodium sulfate nanoparticles with dry diameter 20 (red square) and 6 (blue square) nm, respectively. Black squares and dashed lines show the respective results from Tang et al. (2007) with electrodynamic balance (EDB), respectively. In this study, the black, red, and blue curves show E-AIM predictions, including the Kelvin effect and shape factors ( $\chi$ ).